A Ligand-Directed Approach to Activity-Based Sensing: Developing Palladacycle Fluorescent Probes that Enable Endogenous Carbon Monoxide Detection

Johannes Morstein,[1,2] Denis Höfler,[1] Kohei Ueno,[3] Jonah W. Jurss,[1,4] Ryan R. Walvoord,[1,5] Kevin J. Bruemmer,[1] Samir P. Rezgui,[6] Thomas F. Brewer,[1,7] Minoru Saitoe,[3] Brian W. Michel,*[,1,2,6] Christopher J. Chang*[,1,8,9]

[1]Department of Chemistry, University of California, Berkeley, California 94720, United States. [3]Tokyo Metropolitan Institute of Medical Science, Tokyo, 1568506, Japan. [4]Department of Chemistry and Biochemistry, University of Mississippi, Coulter Hall, University, Mississippi 38677, United States. [5]Department of Chemistry, Ursinus College, 601 E. Main Street, Collegeville, Pennsylvania 19426, United States. [6]Department of Chemistry and Biochemistry, University of Denver, Denver, Colorado, 80210, United States. [7]Genentech Inc., 1 DNA Way, South San Francisco, California 94080, United States. [8]Department of Molecular and Cell Biology, University of California, Berkeley, California 94720, United States. [9]Helen Wills Neuroscience Institute, University of California, Berkeley, California 94720, United States. brian.michel@du.edu; chrischang@berkeley.edu;

[2]These authors contributed equally to this work.

Abstract

Carbon monoxide (CO) is an emerging gasotransmitter and reactive carbon species with broad anti-inflammatory, cytoprotective, and neurotransmitter functions along with therapeutic potential for the treatment of cardiovascular diseases. The study of CO chemistry in biology and medicine relative to other prominent gasotransmitters such as NO and H_2S remains challenging, in large part due to limitations in available tools for the direct visualization of this transient and freely diffusing small molecule in complex living systems. Here we report a ligand-directed activity-based sensing (ABS) approach to CO detection through palladium-mediated carbonylation chemistry. Specifically, the design and synthesis of a series of ABS probes with systematic alterations in the palladium-ligand environment (e.g., sp^3-*S*, sp^3-*N*, sp^2-*N*) establish structure-activity relationships for palladacycles to confer selective reactivity with CO under physiological conditions. These fundamental studies led to the development of an optimized probe, termed Carbon Monoxide Probe-3 Ester Pyridine (**COP-3E-Py**), which enables imaging of CO release in live cell and brain settings, including monitoring of endogenous CO production that triggers presynaptic dopamine release in fly brains. This work provides a unique tool for studying CO in living systems and establishes the utility of a synthetic methods approach to activity-based sensing using principles of organometallic chemistry.

Introduction

Carbon monoxide (CO) is an essential gasotransmitter that exhibits a diverse array of cytoprotective, anti-inflammatory, and signaling effects in living systems.[1–3] In addition to these roles in basic biology, CO is being increasingly recognized for its contributions to medicine as molecules with the capacity to release CO *in vivo*, including Carbon Monoxide Releasing Molecules (CORMs), are being evaluated as potential therapeutics for a broad range of cardiovascular diseases.[4–13] The biological and biomedical importance of CO motivates the need to develop new methods to monitor dynamic changes in CO fluxes with high selectivity and sensitivity in living systems on a molecular level. In this context, fluorescent probes offer a powerful set of chemical reagents for studying other transient biologically active small molecules, including the gasotransmitters NO[14–16] and H_2S[17–27] as well as H_2O_2,[28–43] presaging the use of this approach to decipher the chemistry of CO in biological settings.

As part of a larger program in our laboratory on activity-based sensing (ABS),[44–48] we and others have become interested in developing small-molecule probes for one-carbon species,[49–51] and we reported the development of Carbon Monoxide Probe-1 (**COP-1**),[52] which established the use of palladium-mediated carbonylation chemistry for CO detection with high selectivity over competing reactive oxygen, nitrogen, carbon, and sulfur species. In parallel with our initial report, the He and Chen laboratories described **COSer**,[53] a first-generation fluorescent protein sensor for CO. **COP-1** has been independently applied to monitor and study CO released by CORMs in biological samples[54–57] and its organometallic trigger has been adapted by others to develop various CO-responsive probes,[58–61] including fluorescent indicators for two-photon imaging[62], raman spectroscopy nanosensors,[63] and CO-responsive nanoparticles.[64] In addition, allyl ether-based fluorescent probes have emerged as an alternative strategy for CO-detection,[65–67] but the requirement for exogenous addition of free palladium salts to biological samples makes this 3-component system more challenging to implement. These efforts have spawned broader strategies for exploiting the use of organometallic reactivity in cells.[68–77]

Despite previous successes with **COP-1**, this first-generation ABS probe exhibits shortcomings that limit its broader use in biological settings, including a hydrophobic nature that promotes punctate cellular staining thereby effectively precluding visualization of substantial portions of the cell, as well as relatively poor cellular retention, making washing steps (to increase signal-to-noise responses) in imaging experiments more challenging. We sought to address these issues by turning our attention to studying the underlying fundamental organometallic chemistry of CO detection by systematically modulating the metal-ligand environment of the reactive palladacycle trigger. Specifically, using **COP-1** as a starting point, tuning of the covalently attached amine ligand with sp^3-*S*, sp^3-*N*, sp^2-*N* substitutions and the chloro-dimer-bridge were evaluated to

explore their influence on the reactivity of the CO probe. We adapted the most promising reaction trigger identified in each round of synthetic screening and explored further functionalization of the BODIPY fluorophore to increase aqueous solubility, cellular distribution, and retention properties. These foundational structure-activity studies resulted in the development of an optimized CO-probe, termed Carbon Monoxide Probe-3 Ester Pyridine (**COP-3E-Py**), which exhibits a markedly increased solubility in aqueous media and improved cellular retention. We demonstrate the utility of **COP-3E-Py** for the detection of CO release from CORMs in live cells and brains. Included is the successful visualization of endogenous release of CO during neural stimulation in fly brain preparations using electrical and chemical input, highlighting the potential of fundamental organometallic chemistry for chemical biology applications.

Results and Discussion

Imaging Studies Reveal Differences in Cellular Localization for COP-1 and its Carbonylation COP-1' Product

We initiated structure-activity studies with extensive characterization of **COP-1** and the carboxylic acid product formed from reaction of **COP-1** and CO, termed **COP-1'**. This post-carbonylation product is presumably formed following migratory insertion of **COP-1** with CO to provide a Pd-acyl intermediate and subsequent reductive hydrolysis. Confocal microscopy images of HEK293T cells loaded with **COP-1** showed punctate staining. This phenomenon was revealed to arise from lysosomal localization through a co-staining experiment with lysosome marker **LysoTracker™ Red DND-99**. Interestingly, this experiment showed strong co-localization for **COP-1** with **LysoTracker™ Red DND-99** (PC: 0.792, M1: 0.584) but not for the more polar carboxylic acid product **COP-1'** (PC: 0.600, M1: 0.158) (Figure 1). We initially hypothesized that **COP-1** accumulates in acidic stores due to protonation of the basic directing group.[78] However, while this alkylamine-functionality is shared by **COP-1**, **COP-1'** and **LysoTracker™ Red DND-99** (Figure 1g) the presence of an additional polar carboxyl group on **COP-1'** mitigates lysosomal localization.

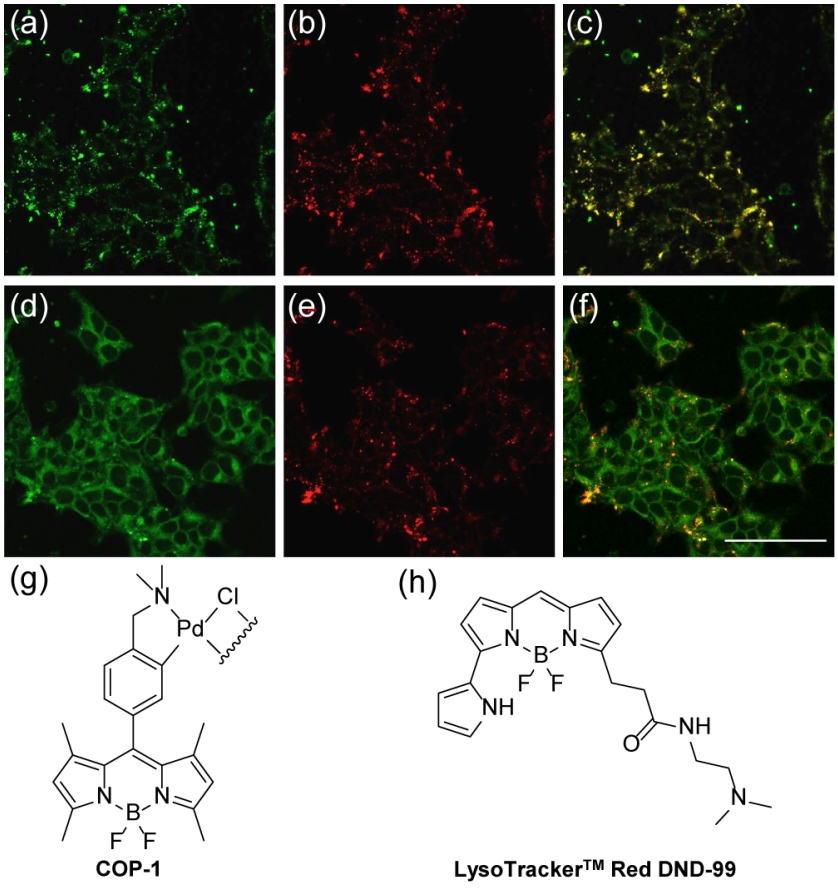

Figure 1. Co-localization of **COP-1** and **COP-1'** with **LysoTracker™ Red DND-99**. (a-c) HEK293T cells were incubated with **COP-1** (1 μM) and **LysoTracker™** (50 nM) for 30 min, resulting in the observed cellular staining of (a) **COP-1**, (b) **LysoTracker™**, and (c) overlay. (d-f) HEK293T cells were incubated with **COP-1'** (1 μM) and **LysoTracker™** (50 nM) for 30 min, resulting in the observed cellular staining of (d) **COP-1'**, (e) **LysoTracker™** and (f) overlay. Scale bar represents 80 μm. (g,h) Chemical structures of **COP-1** and **LysoTracker™ Red DND-99** showing shared alkylamine motifs.

Synthesis, Structure, and CO Reactivity of a Monomeric Analog of COP-1

With data on **COP-1'** showing that a more hydrophilic **COP** analog could promote more even and diffuse cellular staining, we targeted the synthesis of a monomeric **COP** dye in hopes that decreased molecular weight would result in increased hydrophilicity and CO reactivity. To this end, we conducted a bridge-splitting reaction with pyridine as σ-donating ligand to synthesize the monomeric probe **COP-1-Py**.[79] This reaction was conducted with a suspension of **COP-1** in CH_2Cl_2, and upon addition of equimolar amount of pyridine (1:1 with Pd) at room temperature, we observed an immediate increase in solubility in CH_2Cl_2 through the formation of a homogenous solution (Figure 2a). The resulting **COP-1-Py** complex was isolated and behaved similarly *in vitro* to samples prepared from the μ-chloro dimer **COP-1**, reacting with CO to give the same **COP-1'** product. Single crystals of **COP-1**, **COP-1-Py**, and the carbonylation product **COP-1'** were obtained from slow evaporation of concentrated dichloromethane solutions and characterized by single crystal X-ray crystallography to provide molecular connectivity for all three compounds (Figure 2b). As anticipated, the palladacycles of **COP-1** and **COP-1-Py** are perpendicular to the BODIPY plane and the palladium centers adopt a square planar geometry. The crystal structure suggests that **COP-1** exists as a dimer with two μ-chloro bridges linking the palladium(II) centers, whereas **COP-1-Py** exists as a monomer with a single square-planar palladium center. A hydrogen-bonded zwitterion is observed for the **COP-1'** carbonylation product after CO-induced palladium release. The acidic hydrogen of the ammonium group, located in the electron density map, is 1.636 Å from the nearest oxygen of the carboxylate moiety.

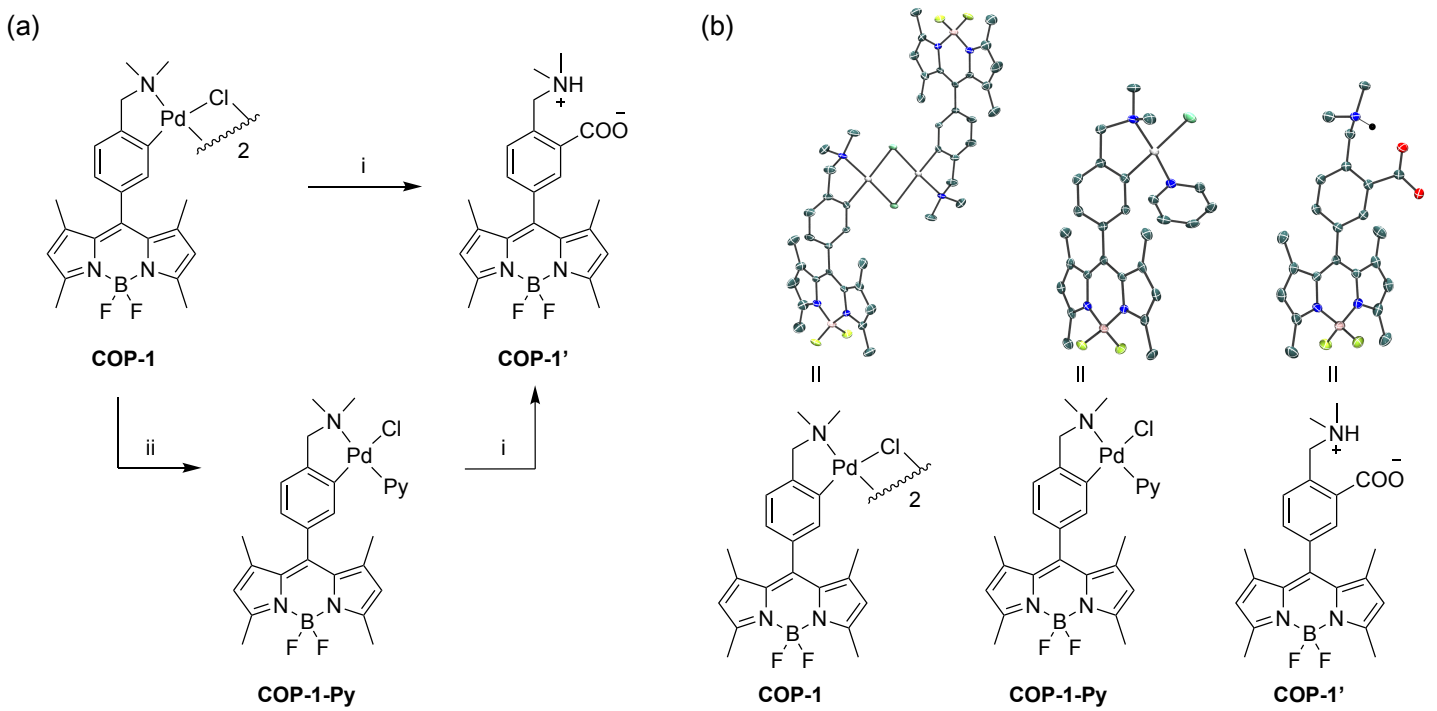

Figure 2. Synthesis and reactivity of the monomeric CO indicator **COP-1-Py** and crystal structures of **COP-1**, **COP-1-Py**, and **COP-1'**. (a) Reagents and conditions: (i) CO, wet CH_2Cl_2, 31 °C, 14 h; (ii) Pyridine, CH_2Cl_2, rt, 5 h, 79%; (b) X-ray crystal structures: hydrogen atoms have been omitted for clarity, except for the H-bonding hydrogen in **COP-1'**. Thermal ellipsoids are shown at the 70% probability level.

Modulation of the Directing Group Ligands on the COP Platform to Tune CO-Dependent Palladacycle Carbonylation Reactivity

Since dimeric **COP-1** and monomeric **COP-1-Py** showed the same CO-dependent carbonylation reactivity, we decided to move forward and design monomeric palladacycles to tune CO reactivity by systematic modulation of the directing group ligand on palladium. In particular, we reasoned that the chelating heteroatom ligand, which is the directing group for the cyclopalladation reaction, does not exhibit fluxional behavior and is therefore expected to potentially have the most profound effect on CO reactivity. We therefore focused our efforts on varying the chelating heteroatom ligand and explored a set of sp^3-*S*, sp^3-*N*, and sp^2-*N* donors. Indeed, these types of directing ligands are known to facilitate the formation of palladacycles and to undergo CO insertion in a biological experimental setting. Whereas carbonylation reactions with palladacycles have been extensively explored in aprotic solvents, we noted that the protic cellular environment could also increase the influence of the directing group's pK_a value on the reactivity of the probe. In addition, we speculated that the protonation state is likely

to affect the subcellular localization of the probe under physiological conditions through different protonation equilibria. We therefore sought to explore directing group ligands spanning several orders of magnitude in pK_a values to evaluate its influence on both reactivity and subcellular localization. Finally, in addition to *N*-basic directing groups, we sought to characterize the potential of an sp^3-*S*-derived palladacycle for CO-sensing applications. Previous mechanistic studies in abiotic reaction environments suggest that these palladacycles undergo more facile CO-insertion compared to sp^3-*N*-derived palladacycles.[79,80] As such, we envisioned that this promotion of CO-insertion could potentially allow for faster reaction kinetics and improved selectivity of the probe scaffold over H_2S, a competing gasotransmitter and a substrate for an off-pathway protodemetallation.

A sp^3-*S*-derived CO-probe, termed **COP-2-Py**, and a comparably less-basic sp^3-*N*-derived morpholino congener to **COP-1**, termed **COP-3-Py**, were obtained via similar synthetic procedures as **COP-1-Py** (Scheme 1). In addition, an oxime-palladacycle probe, **COP-4-Py**, and a pyridine-based dye, **COP-5-Py**, were synthesized via newly developed synthetic routes. (Scheme 1). Specifically, compounds 2 and 3 were prepared in a similar fashion to the **COP-1** precursor, i.e. via a nucleophilic substitution of the benzylic chloride 1. The oxime-containing synthon 7 was prepared from 1,4-phthalaldehyde by mono acetal protection (to differentiate the two aldehydes), BODIPY formation, and acetal hydrolysis to provide aldehyde 6. Condensation with hydroxyl amine then afforded aldoxime 7. 2-Pyridinyl 9 was prepared from the bromo BODIPY 8 via a Stille cross-coupling. All probes were prepared from their precursors via directed palladation, appropriate anion metathesis and bridge-splitting with pyridine.

Scheme 1. Synthesis of COP-2-Py, COP-3-Py, COP-4-Py, and COP-5-Py[a]

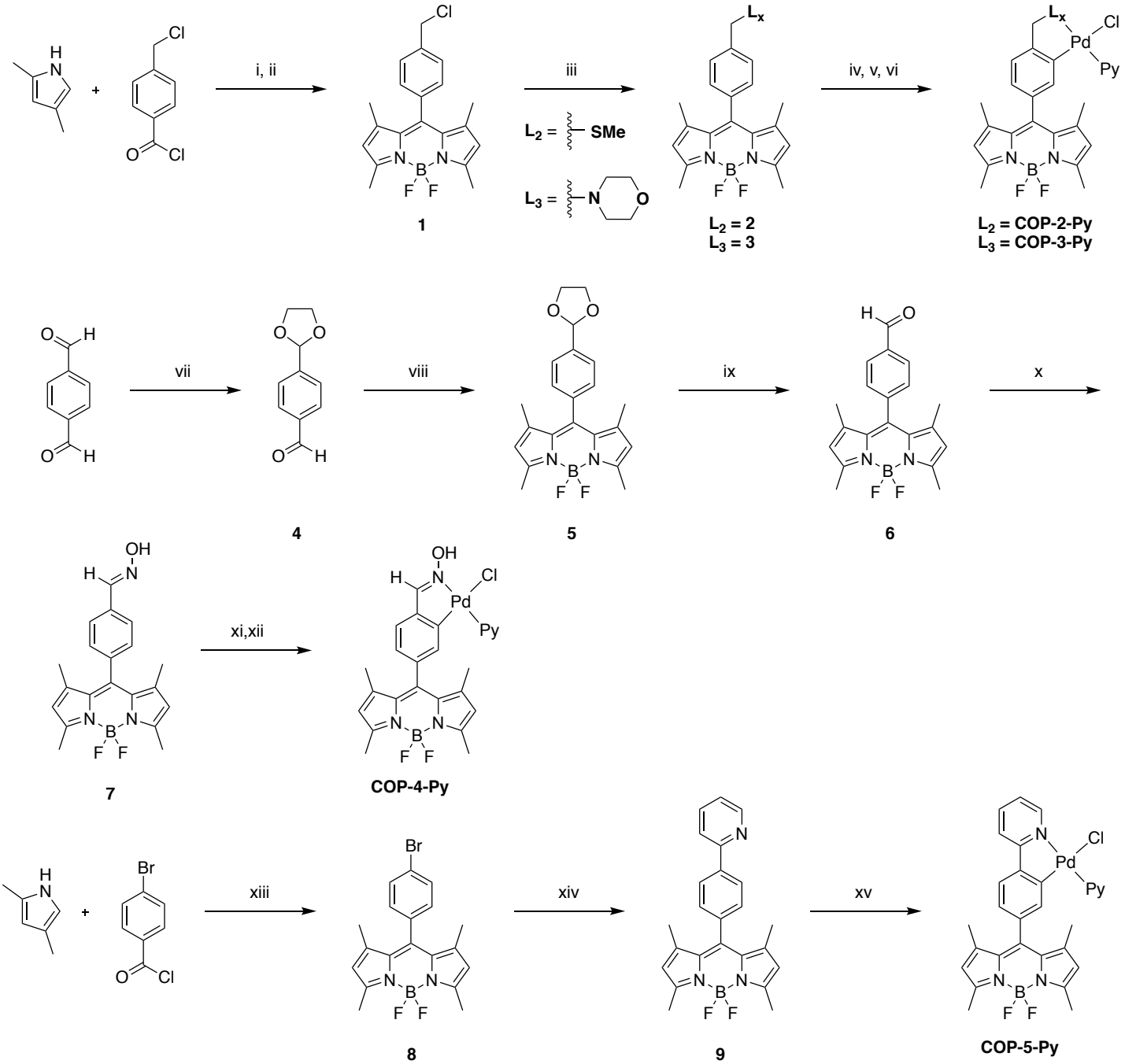

[a]Reagents and conditions: (i) CH_2Cl_2, rt, 14 h; (ii) DIPEA, BF_3•OEt_2, CH_2Cl_2, rt, 3 h, 28% (2 steps); (iii) L_2: NaSMe, EtOH, rt, 25 h, 45%; L_3: KI, K_2CO_3, CH_3CN, morpholine, 80-100 °C, 60 min, 92%; (iv) L_2: $Pd(OAc)_2$, AcOH, 120 °C, 55 min; L_3: $Pd(OAc)_2$, C_6H_6, 50 °C, 14 h; (v) LiCl, acetone, rt, 4 h; (vi) Pyridine, CH_2Cl_2, rt, 5 h, 22% for L_2 (3 steps); 13% for L_3 (3 steps); (vii) ethylene glycol, *p*-toluenesulfonic acid, 130 °C, 4 h, 24%; (viii) 2,4-Dimethylpyrrole, TFA, CH_2Cl_2,16 h, rt, then DIPEA, BF_3•OEt_2, MePh, 45 °C, 50 min, 30%; (ix) Acetone, 10% HCl, reflux, 2 h, 78%; (x) hydroxylamine hydrochloride, KOAc, EtOH, H_2O, 70 °C, 3 h, 91%; (xi) di-μ-chlorobis[2-[(dimethylamino)methyl]phenyl-C,N]-dipalladium(II), $CHCl_3$/AcOH,

50 °C, 16 h; (xii) Pyridine, CH_2Cl_2, rt, 16 h, 69% (2 steps); (xiii) CH_2Cl_2, rt, 14 h, then Et_3N, BF_3•OEt_2, rt, 20 h, 50%; (xiv) 2-(tributylstannyl)pyridine, toluene, $Pd(Ph_3P)_2Cl_2$, 110 °C, 48 h, 65%. (xv) $Pd(OAc)_2$, PhH, 50 °C, 14 h then LiCl, acetone, rt, 4 h then pyridine, CH_2Cl_2, rt, 74%.

With this family of CO probes in hand, we evaluated their comparative reactivity with CO and H_2S *in vitro*, as well as their ability to detect changes in CO levels in live HEK293T cells (Figure 3). Specifically, we evaluated the CO responses of these reagents in buffered aqueous solution using [$Ru(CO)_3Cl$(glycinate)] (CORM-3) as a CO source. **COP-2-Py** did not exhibit a significant fluorescent turn-on response with either CO or H_2S in phosphate buffered saline, suggesting that sp^3-*S*-palladacycles do not undergo facile CO-insertion under physiological conditions relative to sp^3-N-palladacycle congeners. Moreover, **COP-4-Py** and **COP-5-Py** were found to be less chemoselective for CO over H_2S than **COP-1**. Notably, both probes exhibit a stronger relative and absolute fluorescence response with H_2S compared to CO. Whereas **COP-4-Py** shows a continual rise in fluorescence turn-on response with H_2S (over the time course of the experiments), **COP-5-Py** exhibits a rapidly declining fluorescence turn-off response towards H_2S after 15 min. Some possible speculations for this observation are aggregation and/or precipitation of the expected non-polar product from protodemetallation. In contrast to CO, which gives a carbonylated product upon activity-based sensing, H_2S is presumably undergoing protodemetalation due to its acidic nature and potential ability to form a metal-sulfide precipitate.[17] Of this series, **COP-3-Py** exhibits the strongest fluorescence response towards CO with minimal reactivity with H_2S, offering superior specificity over the first-generation **COP-1** reagent. Taken together, these structure-activity relationships for a family of monomeric **COP** dyes suggest that sp^3-*N*-palladacycles appear to be best-suited for the development of palladacycle activity-based sensing probes for CO that achieve improved selectivity over H_2S.

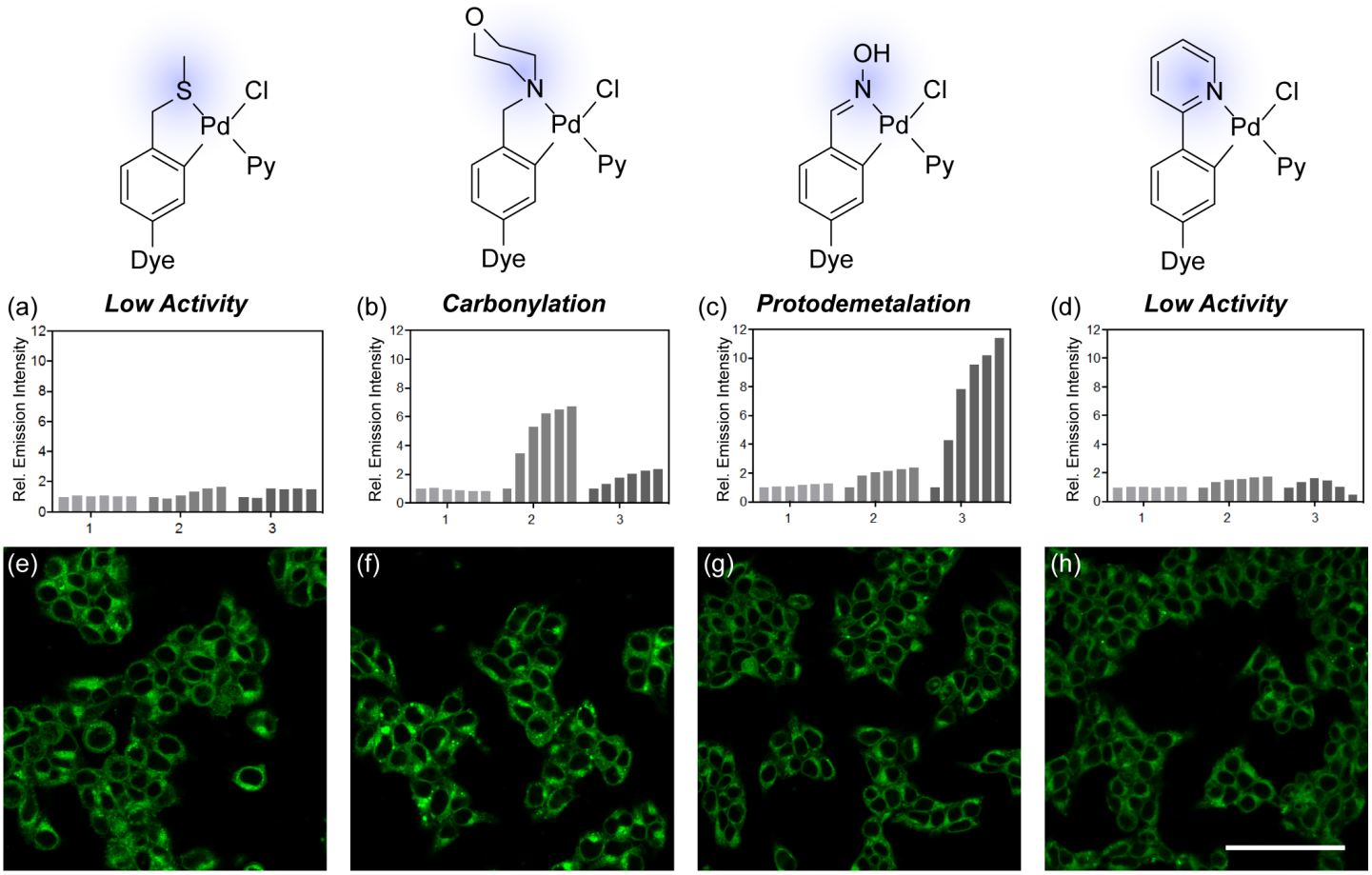

Figure 3. Evaluation of **COP-2-Py**, **COP-3-Py**, **COP-4-Py**, and **COP-5-Py** reactivity *in vitro* and *in cellulo*. (a-d) Fluorescent responses of the respective COP reagent (1 μM) to CO and H_2S. Bars represent integrated fluorescence intensities between 520 and 620 nm normalized to the respective probe in PBS at 0 min. Analytes were incubated at 50 μM concentration in pH 7.4 PBS at 37 °C and the bars correspond to the time points 0, 5, 15, 30, 45 and 60 min after addition of the respective analyte. Legend: (1) control; (2) CO; (3) H_2S. CORM-3 was used as a CO source. (e-h) Cellular staining of the respective probes (1 μM) on a HEK293T cell monolayer after 60 min of incubation show basal localization of the dyes. Scale bar represents 80 μm.

Evaluation of the staining patterns and localizations of all monomeric COP dyes showed observably less punctate staining (Figure 3b, d, f, h) relative to **COP-1** (Figure 1). In addition to making probes less hydrophobic upon reduction in size from dimer to monomer, these results give some indication that less basic directing group ligands can decrease probe localization in acidic stores, presumably by lowering protonation under physiological conditions. However, the sp^3-*N* morpholino analog **COP-3-Py** still exhibits minor punctate staining in HEK293T cells owing to its basic nitrogen donor. As such, we subjected **COP-3-Py** to a second round of structure optimization focusing on the fluorophore backbone.

Synthesis and Characterization of COP-3E-Py Bearing a More Hydrophilic BODIPY Core

The foregoing structure-activity studies led to the identification of a sp^3-*N* morpholino directing ligand on **COP-3-Py** as an improved activity-based sensing trigger for CO detection. To further optimize this scaffold, we next decided to functionalize the BODIPY core with ester chains to increase aqueous solubility and hydrophilicity and improve cellular retention by exploiting native intracellular esterase activity.[81] The probe Carbon Monoxide Probe-3 Ester Pyridine (**COP-3E-Py**) was designed and synthesized according to Scheme 2. Initial deprotection of a commercially available pyrrole gave the more electron-rich pyrrole 10. This intermediate was unstable due to rapid oxidation and was therefore used directly to form BODIPY 11 via condensation with 4-chlorobenzoyl chloride and complexation with BF_3. Nucleophilic substitution of chlorine with morpholine, directed palladium metalation, ligand exchange, and palladacycle-bridge-splitting gave access to the final **COP-3E-Py** probe. The carbonylated product **COP-3E-Py'** was synthesized by reacting **COP-3E-Py** under a CO atmosphere in a solvent mixture of CH_2Cl_2 and water.

Scheme 2. Synthesis of COP-3E-Py and COP-3E-Py'[a]

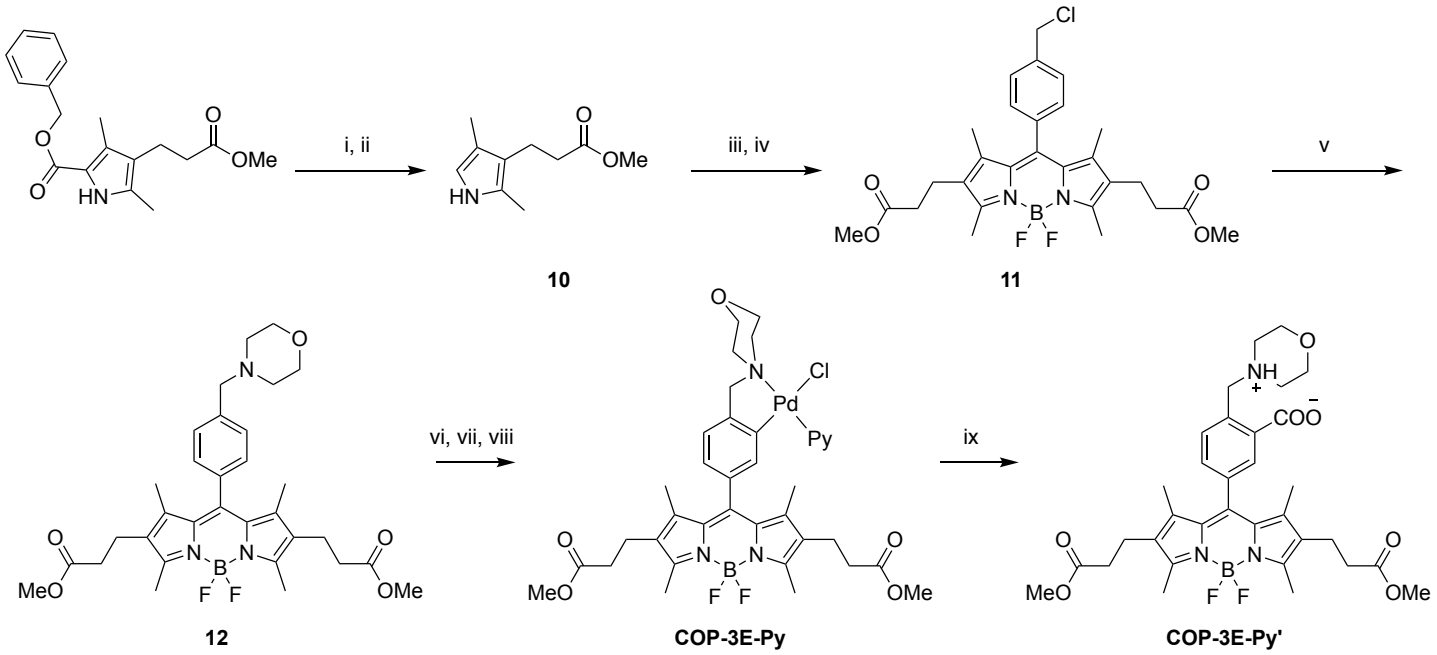

[a]Reagents and conditions: (i) H_2, Pd/C, acetone, rt, 12 h; (ii) TFA, 40 °C, 10 min, 48% (2 steps); (iii) p-(chloromethyl)benzoyl chloride, CH_2Cl_2, rt, 14 h; (iv) DIPEA, BF_3•OEt_2, CH_2Cl_2, rt, 3 h, 22% (2 steps); (v) KI, K_2CO_3, morpholine, CH_3CN, 60 °C, 3 h, 94%; (vi) $Pd(OAc)_2$, C_6H_6, 50 °C, 14 h; (vii) LiCl, acetone, rt, 4 h; (viii) Pyridine, CH_2Cl_2, rt, 5 h, 70% (3 steps); (ix) CO, wet CH_2Cl_2, 31 °C, 14 h, 92%.

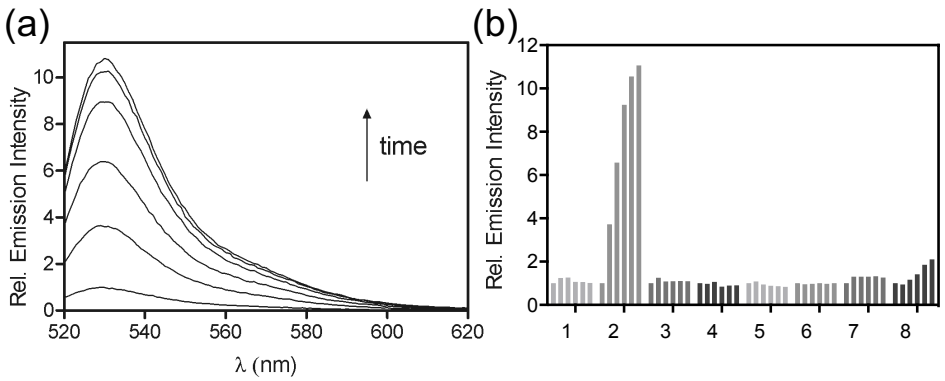

Figure 4. Turn-on fluorescence response to CO and analyte selectivity of **COP-3E-Py** in buffered aqueous solution. (a) Turn-on fluorescence response of **COP-3E-Py** (1 μM) to CORM-3 (50 μM) in pH 7.4 PBS at 37 °C (λ_{ex} = 515 nm, emission collected from 520 – 630 nm). Time points taken at 0, 5, 15, 30, 45 and 60 min after addition of CORM-3. (b) Fluorescence responses of **COP-3E-Py** (1 μM) to CO and other biologically relevant reactive small molecules. Bars represent integrated fluorescence intensity between 520 and 620 nm normalized to **COP-3E-Py** in PBS at 0 min. Analytes were incubated at 50 μM concentration in pH 7.4 PBS at 37 °C and the bars correspond to the time points 0 (or 1 for (8)), 5, 15, 30, 45 and 60 min after addition of the respective analyte. Legend: (1) control; (2) CORM-3; (3) H_2O_2; (4) NaOCl; (5) TBHP; (6) KO_2; (7) $ONOO^-$; (8) H_2S.

In aqueous PBS solution we observed an 11-fold fluorescence turn-on for **COP-3E-Py** (1 μM) upon addition of CORM-3 (50 μM) as a CO source within 60 min. Both the **COP-3E-Py** indicator (λ_{max} = 521 nm, λ_{em} = 535 nm, Φ_{fl} = 0.12, ε_{521} = 31000 $M^{-1}cm^{-1}$) and its carbonylated product **COP-3E-Py'** (λ_{max} = 521 nm, λ_{em} = 537 nm, Φ_{fl} = 0.51, ε_{521} = 43000 $M^{-1}cm^{-1}$) exhibit a red shift compared to the parent **COP-1** (λ_{max} = 499 nm, λ_{em} = 503 nm). Other potentially competing analytes, including reactive nitrogen, oxygen, and sulfur species, were tested at the same concentration (50 μM) for reactivity with **COP-3E-Py** (Figure 4). Only minimal responses were observed with other biologically relevant small molecules in this assay, showing the high specificity for activity-based sensing of CO by the **COP-3E-Py** palladacycle.

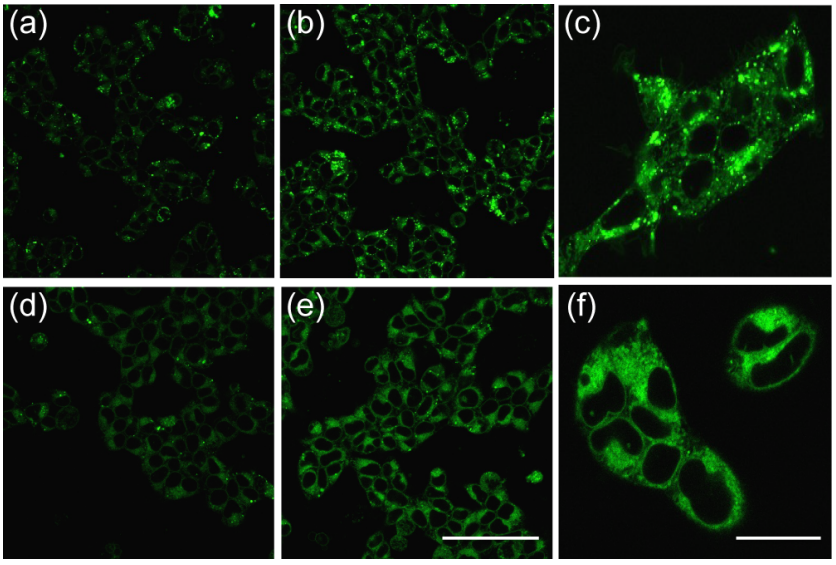

Figure 5. Live-cell imaging comparison between **COP-1** and **COP-3E-Py** establishing improved diffuse staining of the more hydrophilic **COP-3E-Py** congener compared to lysosomal localization of **COP-1**. (a,b,d,e) CO-detection in live HEK293T cells using **COP-3E-Py** and **COP-1**. HEK293T cells were incubated with 1 μM **COP 1** (a,b) or **COP-3E-Py** (d,e) for 120 min total, with negative control vehicle or **CORM-3** (50 μM) added for the positive control for the final 60 min (b,e). (c,f) Representative images taken at 63x for staining pattern comparison. Scale bar represents 80 μm (a,b,d,e) or 20 μm (c,f).

We next evaluated the ability of **COP-3E-Py** to image CO in biological samples and compared its performance to **COP-1**. Administration of **CORM-3** to live HEK293T cells in the presence of **COP-1** or **COP-3E-Py** yielded a robust fluorescent turn-on response in both cases (Figure 5). However, in contrast to **COP-1**, which accumulated in lysosomes, **COP-3E-Py** gave a more diffuse, homogeneous staining pattern in live cells. Moreover, dual-dye imaging experiments with **COP-3E-Py** and **ER-Tracker Red E34250** in the presence of CO indicate some co-localization with the ER (PC: 0.913, M1: 0.682, Figure 6).[9] Notably, the observation that this CO detection reagent can monitor changes in CO fluxes associated with the ER is desirable owing to the ER-membrane localization of heme oxygenase-1 (HO-1) which a major endogenous source for production of CO.[82] As such, the increased hydrophilicity of **COP-3E-Py** relative to **COP-1** affords improved detection of CO through broader distribution of the probe throughout the cell.

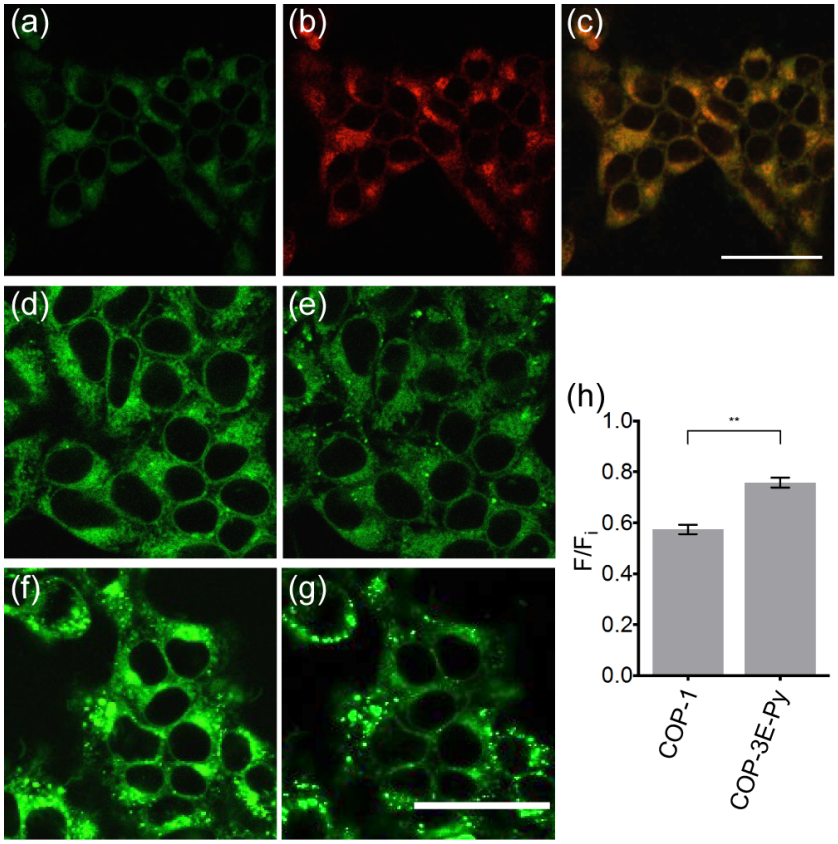

Figure 6. Live-cell imaging comparison between **COP-3E-Py** and **COP-1** reagents showing superior retention of the **COP-3E-Py** dye after sample washing. Panels (a-c) show subcellular localization of **COP-3E-Py**. HEK293T cells were stained with **COP-3E-Py** (a, 1 μM) and ER-Tracker Red E34250 (b, 1 μM). (d-g) Confocal microscopy images of HEK293T cells with **COP-3E-Py** (d,e) or **COP-1** (f,g) were taken before and after a buffer exchange was conducted. The images after buffer-exchange were recorded after an equilibration period of 10 min. (h) Mean fluorescence intensities of images acquired 10 min after buffer exchange as fractions of the initial fluorescence before buffer exchange. Error bars denote SEM (n = 3). **P < 0.002. Scale bars represent 40 μm (for a-c and d-g).

Next, we conducted comparative cellular retention assays with **COP-1** and **COP-3E-Py** (Figure 6). Probes were loaded into cells and imaged, and then washed by a buffer exchange and imaged again. Under these conditions, the fraction of final fluorescence intensity relative to initial fluorescence intensity of **COP-1** was 57%, with **COP-3E-Py** offering an improvement to 76% retention of fluorescence signal after washing (Figure 6). The observed increase in cellular retention for **COP-3E-Py** expands opportunities for using this reagent for CO detection in biological settings that benefit from protocols with washing steps. These data establish that systematic modification of the activity-based sensing palladacycle trigger for

selective tuning of CO reactivity as well as increasing hydrophilicity of the BODIPY core for improved cellular localization and retention leads to **COP-3E-Py** as an advanced reagent for biological CO detection with enhanced properties.

COP-3E-Py Enables Detection of Endogenous CO Release in Fly Brain Models

To showcase the utility of palladacycle **COP-3E-Py** for biological CO imaging applications, we sought to apply this reagent to observe endogenous CO signaling events. To this end, we utilized **COP-3E-Py** to monitor the postsynaptic release of CO in a fly brain model, as a novel role for CO as a retrograde messenger in noncanonical dopamine release was recently established.[83] Fly brains were isolated and the mushroom body vertical lobes were imaged with **COP-3E-Py**, with a washing step after probe incubation (Figure 7). Two different types of stimulation were employed to evoke dopamine release and neurotransmission in this biological model: (1) electrical stimulation of the antennal lobe, and (2) bath application with NMDA. A clear increase in **COP-3E-Py** fluorescence was observed, confirming that this probe could monitor endogenous CO release mediated in this fly brain region.

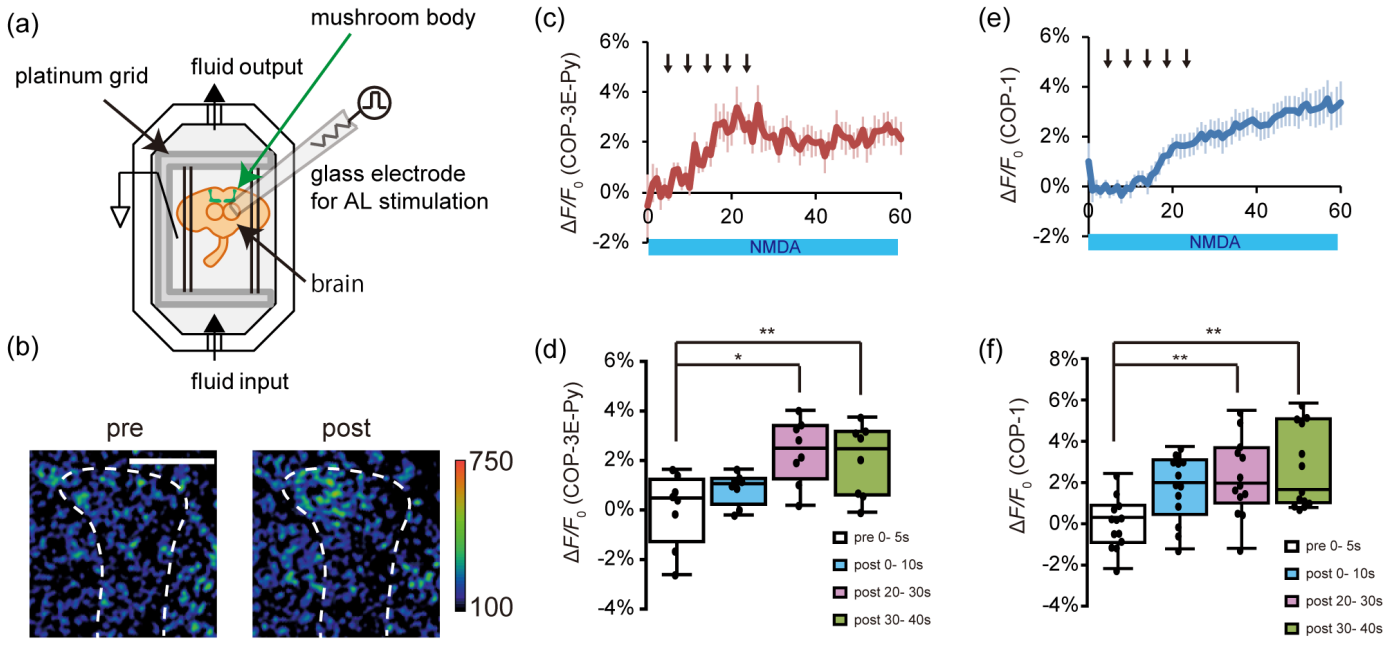

Figure 7. Endogenous CO release monitored with **COP-3E-Py**. (a) Schematic of the fly brain experiment. (b) Representative images of **COP-3E-Py** fluorescence observed at the α3/α'3 compartments of the mushroom body vertical lobes of the fly brain preparation. Scale bar represents 25 μm. (c-f) Trace and quantification of turn-on response after stimulation of the

antennal lobe and NMDA stimulation using **COP-3E-Py** or **COP-1** respectively. *p < 0.05; **p < 0.01; Bonferroni *post hoc* test.

Concluding Remarks

In summary, we have presented a ligand-directed approach to activity-based sensing of CO using organometallic reactivity. In-depth evaluation of the first-generation palladacycle probe **COP-1** and systematic modulation of the ligand environment on palladacycle reactivity under physiological conditions laid a foundation for the development of next-generation molecular imaging probes for biological CO. The data revealed that sp^3-*N*-palladacycles are superior to other common classes of palladacycles investigated. Remarkably, sp^3-*N*-palladacycles undergo facile CO insertion and are also sufficiently stable towards protodemetallation under physiological conditions as shown by comparative reactivity studies with the competing gasotransmitter H_2S. Further functionalization of the core BODIPY fluorophore with hydrophilic ester substituents gave rise to the development of **COP-3E-Py**, an optimized scaffold with improved properties for CO detection, including more diffuse cellular staining and enhanced cellular retention. This advanced CO probe enabled detection of biological CO in both cell and fly brain models, as shown by monitoring **CORM-3**-mediated CO release in live HEK293T cells and visualization of endogenous CO release in fly brain preparations upon electrical and NMDA stimulation. In addition to providing a unique chemical tool for deciphering biological and biomedical contributions of CO, this study provides a starting point for the broader use of organometallic principles in the design of activity-based sensing probes for chemical biology applications.

Experimental Section

General Methods. Reactions utilizing air- or moisture sensitive reagents were performed in oven- or flame-dried glassware under an atmosphere of dry N_2. Reagents from commercial sources were used as received without further purification. Reagents were purchased from Sigma-Aldrich (St. Louis, MO). All solvents were of reagent grade. COP-1,[52] COP-1',[52] and CORM-3[84] were synthesized according to literature procedures. Silica gel P60 (SiliCycle) was used for all column chromatography purifications and SiliCycle 60 F254 silica gel (precoated sheets, 0.25 mm thick) was used for thin layer chromatography. ^{1}H and ^{13}C NMR spectra were acquired at 25°C with Bruker AVB-400, AVQ-400, or AV-300 at the College of Chemistry NMR facility at UC Berkeley (UCB). Signals were internally calibrated to solvent peaks. High resolution mass spectrometry (ESI-MS) data were provided by the mass spectrometry department of UCB.

Synthesis of COP-1-Py. A round bottom flask was charged with COP-1 (78.3 mg, 0.15 mmol, 1 eq). CH_2Cl_2 (15 mL) and pyridine (14.5 µL, 0.18 mmol, 1.2 eq) were added and the solution was stirred for 4 h. Hexanes was added and the precipitate was collected with a Büchner funnel to yield COP-1-Py (80.9 mg, 0.15 mmol, 98%) as an orange solid. ^{1}H-NMR (400 MHz, $CDCl_3$): δ 8.77 (d, *J* = 5.4 Hz, 2H), 7.78 (t, *J* = 7.9 Hz, 1H), 7.36 – 7.29 (m, 2H), 7.09 (d, *J* = 7.5 Hz, 1H), 6.88 (d, *J* = 7.3 Hz, 1H), 5.93 (s, 2H), 5.92 (s, 1H), 4.06 (s, 2H), 2.94 (s, 6H), 2.50 (s, 6H), 1.42 (s, 6H).

Synthesis of 1. 4-(Chloromethyl)benzoyl chloride (5.00 g, 26.5 mmol, 1.0 equiv.) was dissolved in dry CH_2Cl_2 (350 mL) and the solution was sparged with N_2 for 40 min. 2,4-dimethylpyrrole (6.80 mL, 66.1 mmol, 2.5 equiv.) was added and the mixture was stirred for 16 h at rt. Dry diisopropylethylamine (23.0 mL, 132 mmol, 5.0 equiv.) was added within 1 min and stirring was continued at room temperature for 15 min. BF_3•OEt_2 was added dropwise to the flask and the mixture was allowed to stir at room temperature for 15 min. The flask was then equipped with a water-cooled condenser and heated to 50 °C for 50 min. The mixture was then allowed to cool to room temperature and concentrated *in vacuo*. The resulting residue was dissolved in CH_2Cl_2, washed with water, dried over Na_2SO_4, filtered and concentrated *in vacuo*. Purification with flash chromatography on silica gel eluting with CH_2Cl_2:Hexanes (50:50 → 60:40 → 75:25) to provide **1** (2.74 g, 7.35 mmol, 28%) as an orange solid. ^{1}H-NMR (400 MHz, $CDCl_3$) spectrum showed accordance with the literature.[52] ^{1}H-NMR (400 MHz, $CDCl_3$): δ 7.52 (d, J = 8.1 Hz, 2H), 7.26 (d, J = 8.1 Hz, 1H), 5.99 (s, 2H), 4.66 (s, 2H), 2.56 (s, 6H), 1.38 (s, 6H).

Synthesis of 2. 1 (558 mg, 1.50 mmol, 1.0 equiv) and NaSMe (210 mg, 3.00 mmol, 2.0 equiv) were dissolved in EtOH under N_2 atmosphere. The mixture was stirred for 25 h at rt. It was diluted with CH_2Cl_2, washed with H_2O, dried over Na_2SO_4,

filtered and concentrated *in vacuo*. Purification with flash column chromatography with CH_2Cl_2:Hexanes (60:40 → 100:0) yielded **2** (259 mg, 0.68 mmol, 45%) as a red solid. NMR: ^{1}H NMR (600 MHz, $CDCl_3$) δ 7.42 (d, *J* = 7.5 Hz, 2H), 7.22 (d, *J* = 7.6 Hz, 2H), 5.97 (s, 2H), 3.74 (s, 2H), 2.54 (s, 6H), 1.96 (s, 3H), 1.38 (s, 6H). ^{13}C NMR (151 MHz, $CDCl_3$) δ 155.54, 143.10, 141.59, 139.30, 133.73, 131.54, 129.81, 128.18, 121.32, 38.01, 14.47. HRMS(ESI) calcd. for $C_{21}H_{23}BF_2N_2S$ [M]: 384.1638; found: 384.1633.

Synthesis of COP-2-Py. A round bottom flask equipped with a water condenser was charged with **2** (50.0 mg, 0.130 mmol, 1.05 equiv.) and $Pd(OAc)_2$ (27.8 mg, 0.124 mmol, 1 equiv.) under a nitrogen atmosphere. AcOH (2 mL) was added. The mixture was stirred in an oil bath at 120 °C for 55 min and then allowed to cool to room temperature. CH_2Cl_2 (10 mL) was added and the solution was washed with H_2O (15 mL x 2). The organic layer was collected and concentrated *in vacuo*. The resulting crude solid was dissolved in a saturated solution of LiCl in acetone (3 mL) and was allowed to stir for 30 min at room temperature. Acetone was removed *in vacuo* and the residue was dissolved in CH_2Cl_2. The mixture was passed through a plug of celite and concentrated, yielding an orange solid. The solid was redissolved in minimal CH_2Cl_2 and hexanes were added. The resulting precipitate was collected by vacuum filtration to provide COP-2 (39 mg, 0.037 mmol). This material was suspended in minimal CH_2Cl_2. Pyridine (2.1 equiv relative to Pd) was added and the reaction mixture was allowed to stir for 5 min. CH_2Cl_2 was removed *in vacuo*, and the excess pyridine was removed by azeotroping with CH_2Cl_2 (x5). The resulting orange solid was collected in minimal CH_2Cl_2 and hexanes was added. The resulting precipitate was collected by vacuum filtration, to yield COP-2-Py (15 mg, 22%) as an orange solid. ^{1}H NMR (400 MHz, Chloroform-*d*) 8.77 (d, *J* = 5.8 Hz, 2H), 7.81 (m, 1H), 7.37 (m, 2H), 7.18 (d, *J* = 7.8 Hz, 1H), 6.87 (d, *J* = 7.7 Hz, 1H), 6.14 (s, 1H), 5.93 (s, 2H), 4.38 (d, *J* = 14.2 Hz, 1H), 4.12 (d, *J* = 14.1 Hz, 1H), 2.74 (s, 3H), 2.49 (s, 6H), 1.41 (s, 3H), 1.38 (s, 3H). δ 155.3, 155.0, 153.4, 153.0, 152.4, 148.7, 143.2, 142.5, 142.2, 138.9, 133.5, 132.7, 131.4, 131.3, 125.6, 125.0, 124.3, 123.8, 121.1, 120.9, 48.6, 34.7, 25.3, 23.0, 20.7, 14.5. HRMS(ESI) calcd. for $C_{25}H_{28}BF_2N_4PdS$ [M-Cl-Py+2MeCN]: 571.1131; found: 571.1124.

Synthesis of 3. 1 (0.222 g, 0.596 mmol, 1.0 equiv.), KI (0.198 g, 1.19 mmol, 2.0 equiv.), and K_2CO_3 (0.165 mg, 1.19 mmol, 2.0 equiv.) were suspended in CH_3CN (1.8 mL) and morpholine (260 µL, 2.98 mmol, 5.0 equiv.) was added. The reaction mixture was heated via microwave irradiation to 80 °C for 5 min, then to 100 °C for 60 min and cooled to room temperature. The mixture was diluted with CH_2Cl_2 (60 mL), washed with water, brine, dried over Na_2SO_4, filtered and concentrated *in vacuo*. Purification with flash chromatography on silica gel eluting with a 4:1 mixture of hexanes/CH_2Cl_2 and running a shallow gradient from 0 to 5% EtOAc in this mixture yielded **3** (0.325 g, 0.768 mmol, 92%) as an orange solid. ^{1}H-NMR (600 MHz, $CDCl_3$): δ 7.45 (d, J = 7.7 Hz, 2H), 7.22 (d, J = 7.8 Hz, 2H), 5.96 (s, 2H), 3.73 (t, J = 4.6 Hz, 4H), 3.59 (s, 2H), 2.54 (s,

6H), 2.46 (t, J = 4.5 Hz, 4H), 1.36 (s, 6H). ^{13}C NMR (151 MHz, $CDCl_3$): δ 155.3, 142.9, 141.6, 138.6, 133.8, 131.4, 129.8, 127.9, 121.1, 121.1, 66.9, 62.9, 53.5, 14.5, 14.3. HRMS(ESI) calcd. for $C_{24}H_{29}BF_2N_3O^+$ $[M+H]^+$: 424.2366; found: 424.2365.

Synthesis of COP-3-Py. Amine **3** (0.212 g, 0.501 mmol, 1.05 equiv.), $Pd(OAc)_2$ (0.107 g, 0.477 mmol, 1.00 equiv.), and benzene (5 mL) were added to a 20 mL vial under an atmosphere of N_2. The mixture was heated to 50 °C in an oil bath under stirring for 16 h. The solution was cooled to room temperature, concentrated *in vacuo*. The mixture was then dissolved in CH_2Cl_2 and filtered over a fritted funnel and concentrated *in vacuo*. 5 mL of a saturated LiCl solution in acetone was added and the reaction mixture was stirred for 16 h. The reaction mixture was filtered over a fritted funnel with CH_2Cl_2 and methanol, concentrated in *vacuo* and dissolved in CH_2Cl_2 (5 mL). Pyridine (81.0 µL, 1.00 mmol, 2.00 equiv.) was added and the reaction mixture was stirred 16 h at room temperature. The reaction mixture was concentrated *in vacuo*, suspended in CH_2Cl_2 and filtered over a Büchner funnel. Addition of hexanes led to the precipitation of a solid which was collected. This solid was again precipitated with CH_2Cl_2 and hexanes. The generated solids were again collected. The solids were dissolved in CH_2Cl_2 and filtered over a Büchner funnel. The mother liquor was concentrated *in vacuo* to provide COP3-Py as an orange solid (0.043 g, 0.063 mmol, 13%).[52] ^{1}H-NMR (400 MHz, $CDCl_3$): δ 8.90 - 8.79 (m, 2H), 8.78 - 8.70 (m, 2H), 7.77 (dddt, J = 7.5, 5.7, 3.7, 1.8 Hz, 2H), 7.33 (tdd, J = 10.5, 5.7, 1.4 Hz, 4H), 7.13 (d, J = 7.6 Hz, 1H), 6.89 (dd, J = 7.5, 1.6 Hz, 1H), 5.92 (s, 2H), 4.43 (s, 2H), 4.10 (ddt, J = 9.8, 7.3, 3.2 Hz, 4H), 3.99 - 3.85 (m, 2H), 2.84 (dt, J = 13.6, 4.3 Hz, 2H), 2.49 (s, 6H), 1.39 (s, 6H). ^{13}C NMR (101 MHz, CD_3OD) δ 155.1, 153.3, 153.1, 150.1, 146.5, 142.7, 142.4, 138.6, 138.5, 132.1, 131.3, 130.7, 125.4, 124.9, 124.2, 122.5, 120.9, 68.1, 62.4, 58.8, 14.5, 14.4, 14.3. HRMS(ESI) calcd. for $C_{34}H_{38}BF_2N_5OPd$+ [M+H]+: 687.2167; found 687.2167.

Synthesis of 4. A round-bottom flask was charged with terephthalaldehyde (25.5 g, 190 mmol, 1.00 equiv.), ethylene glycol (11.2 mL, 200 mmol, 1.05 equiv.), toluene (300 mL) and *p*-toluenesulfonic acid (1.81 g, 9.5 mmol, 0.05 equiv.). A Dean-Stark trap was attached and the reaction mixture was refluxed at 130 °C on an oil bath for 4 h. The oil bath was removed and the reaction mixture was concentrated under reduced pressure. The crude product was purified via flash chromatography on silica gel eluting with 20% CH_2Cl_2, 80% hexanes → 20% CH_2Cl_2, 12% ethyl acetate, 68% hexanes → 20% CH_2Cl_2, 16% ethyl acetate, 64% hexanes. The product mixture was refined with a second round of flash chromatography on silica gel eluting with 100% CH_2Cl_2 providing the desired product (8.20 g, 46.0 mmol, 24%) as a colorless liquid. Not all product containing fractions were further purified from the unprotected and diprotected mixture. An acquired ^{1}H-NMR (600 MHz, $CDCl_3$) spectrum showed accordance to the literature.[85] ^{1}H-NMR (400 MHz, $CDCl_3$): δ 10.04 (s, 1H), 7.91 (d, J = 8.2 Hz, 2H), 7.66 (d, J = 8.1 Hz, 2H), 5.88 (s, 1H), 4.24 - 3.95 (m, 4H).

Synthesis of 5. A two-necked round-bottom flask was charged with dry CH_2Cl_2 (500 mL) which was sparged with N_2 for 15 min. Aldehyde **4** (2.07 g, 11.6 mmol, 1.0 equiv.), 2,4-Dimethylpyrrole (2.51 mL, 24.4 mmol, 2.1 equiv.), and 1 drop of trifluoroacetic acid was added. The reaction mixture was stirred 16 h at room temperature. A slurry of 2,3-dichloro-5,6-dicyano-1,4-benzoquinone (2.63 g, 11.6 mmol, 1.0 equiv.) in dry CH_2Cl_2 (150 mL) was added to the reaction mixture. Stirring was then continued for 60 min. The reaction mixture was concentrated *in vacuo* until approximately 100 mL of solvent were left. Dry toluene (300 mL) and dry diisopropylethylamine (10.1 mL, 58.0 mmol, 5.0 equiv.) were added. BF_3•OEt_2 (7.16 mL, 58.0 mmol, 5.0 equiv.) was added and the mixture was heated up to 50 °C in an oil bath for 45 min. The oil bath was removed and the reaction mixture was concentrated *in vacuo*. The crude solid was dissolved in CH_2Cl_2, washed three times with H_2O, dried over Na_2SO_4, filtered over Celite and concentrated *in vacuo*. Purification via flash chromatography on silica gel eluting with 60% CH_2Cl_2, 40% hexanes → 100% CH_2Cl_2 provided BODIPY **5** (1.39 g, 3.51 mmol, 30%) as an orange solid. ^{1}H-NMR (400 MHz, $CDCl_3$): δ 7.61 (d, J = 7.9 Hz, 2H), 7.31 (d, J = 7.8 Hz, 2H), 5.97 (s, 2H), 5.85 (s, 1H), 4.24 - 4.13 (m, 2H), 4.13 - 4.01 (m, 2H), 2.55 (s, 6H), 1.36 (s, 6H). ^{13}C NMR (101 MHz, $CDCl_3$): δ 155.5, 143.1, 141.1, 138.8, 135.9, 131.3, 128.0, 127.4, 121.2,103.3, 65.4, 14.5, 14.5. HRMS(ESI) calcd. for $C_{22}H_{23}BF_2N_2NaO^+$ $[M+Na]^+$ 419.1713; found 419.1715

Synthesis of 6. A 100 mL round-bottom flask equipped with a water-cooled condenser was charged with BODIPY **5** (0.793 g, 2.00 mmol, 1.0 equiv.), acetone (20 mL) and a 10% HCl (aq.) solution (1.0 mL). The reaction mixture was put under N_2 and refluxed on an oil bath for 2 h. The oil bath was removed and the reaction mixture was concentrated *in vacuo*. The resulting residue was dissolved in CH_2Cl_2 and the organic phase was washed three times with H_2O, dried over Na_2SO_4, filtered over Celite, and concentrated *in vacuo*. Purification via flash chromatography on silica gel eluting with 60% CH_2Cl_2, 40% hexanes → 100% CH_2Cl_2 provided aldehyde **6** (0.554 g, 1.57 mmol, 78%) as an orange solid.[85] ^{1}H-NMR (400 MHz, $CDCl_3$): δ 10.10 (s, 1H), 8.02 (d, J = 7.8 Hz, 2H), 7.49 (d, J = 7.8 Hz, 2H), 5.99 (s, 2H), 2.55 (s, 6H), 1.34 (s, 6H). ^{13}C NMR (101 MHz, $CDCl_3$) δ 191.5, 156.1, 142.7, 141.3, 139.6, 136.6, 130.7, 130.3, 129.0, 121.6, 14.6, 14.5. HRMS(ESI) calcd. for $C_{20}H_{20}BF_2N_2O^+$ $[M+H^+]$ 353.1631; found 353.1629

Synthesis of 7. A round-bottom flask equipped with a water cooled condenser was charged with hydroxylamine hydrochloride (0.160 g, 2.30 mmol, 3.0 equiv.), potassium acetate (0.340 g, 3.45 mmol, 4.5 equiv.), ethanol (10 mL), H_2O (5 mL), and aldehyde **6** (0.280 g, 0.795 mmol, 1.0 equiv.). The reaction mixture was put under N_2 and heated up to 70 °C in an oil bath for 3 h. The oil bath was removed and the reaction mixture was concentrated *in vacuo*. The resulting residue

was dissolved in CH_2Cl_2 and concentrated *in vacuo*. CH_2Cl_2 was added and the organic phase was washed one time with H_2O, dried over Na_2SO_4, filtered over Celite, and concentrated *in vacuo*. Purification via flash chromatography on silica gel eluting with 100% CH_2Cl_2 → 5% ethyl acetate, 95% CH_2Cl_2 provided aldoxime **7** (0.266 g, 0.724 mmol, 91%) as an orange solid. ^{1}H-NMR (400 MHz, $CDCl_3$): δ 8.21 (s, 1H), 7.72 (d, J = 8.2 Hz, 2H), 7.32 (d, J = 8.1 Hz, 2H), 5.99 (s, 2H), 2.56 (s, 6H), 1.40 (s, 6H). ^{13}C NMR (101 MHz, Acetone-d6): δ 156.2, 148.8, 143.8, 142.4, 136.5, 135.0, 131.9, 129.3, 128.2, 122.1, 122.1, 14.7, 14.6, 14.6, 14.6. HRMS(ESI) calcd. for $C_{20}H_{21}BF_2N_3O^+$ $[M+H]^+$ 368.1740; found 368.1739

Synthesis of COP-4-Py. A two-necked round-bottom flask equipped with a water-cooled condenser was charged with aldoxime **7** (0.119 g, 0.325 mmol, 1.0 equiv.) and di-μ-chlorobis[2-[(dimethylamino)methyl]phenyl-C,N]dipalladium(II) (0.090 g, 0.163 mmol, 1.0 equiv.). The mixture was dissolved in a 1:1 solution of $CHCl_3$/acetic acid (20 mL). The reaction mixture was heated to 50 °C in an oil bath for 16 h under stirring. The oil bath was removed and the precipitates were collected on a Büchner funnel. The solids were transferred to a 20 mL vial and dissolved in 10 mL CH_2Cl_2. Pyridine (52 μL, 0.65 mmol, 2.0 equiv.) was added and the reaction mixture was stirred for 16 h at room temperature, filtered over Celite, concentrated to 5 mL and hexanes (5 mL) was added, which lead to immediate precipitation. The precipitate was collected with a Büchner funnel to yield **COP-4-Py** (0.131 g, 0.223 mmol, 69%) as an orange solid. ^{1}H-NMR (500 MHz, $CDCl_3$): δ 10.20 (s, 1H), 8.78 - 8.70 (m, 2H), 7.91 (s, 1H), 7.87 (tt, J = 7.7, 1.7, 1H), 7.49 - 7.41 (m, 2H), 7.32 (d, J = 7.6, 1H), 6.98 (dd, J = 7.6, 1.6, 1H), 6.15 (d, J = 1.5, 1H), 5.94 (s, 2H), 2.49 (s, 6H), 1.43 (s, 6H). ^{13}C NMR (126 MHz, $CDCl_3$): δ 156.3, 155.4, 153.6, 152.5, 142.8, 142.4, 141.2, 139.0, 135.1, 130.9, 130.1, 126.3, 126.2, 124.7, 121.1, 14.5, 14.5. HRMS(ESI) calcd. for $C_{25}H_{25}BClF_2N_4OPd^+$ $[M+H]^+$ 587.0807; found 587.0807

Synthesis of 8. 4-Bromobenzoylchloride (6.14 g, 26.3 mmol, 1 equiv) was dissolved in dry CH_2Cl_2 (65 mL) in a N_2-atmosphere. 2,4-dimethylpyrrole (5.04 g, 53.0 mmol, 2 equiv) were added and reaction mixture was stirred for 14 h at room temperature. Triethylamine (11.0 mL, 78.3 mmol, 3 equiv) was added dropwise and stirred for 15 min. $BF_3{\cdot}OEt_2$ (17.0 mL, 137 mmol, 5.3 equiv) was added dropwise and the reaction mixture was stirred for 20 h. CH_2Cl_2 was added, the organic layer was washed with water, dried over Na_2SO_4 and concentrated *in vacuo*. The product was purified by flash chromatography on silica gel, eluting with 50% CH_2Cl_2 in Hexanes. ^{1}H NMR (400 MHz, $CDCl_3$): δ 7.63 (d, *J* = 7.9 Hz, 2H), 7.14 (d, *J* = 8.0 Hz, 2H), 5.99 (s, 2H), 2.54 (s, 6H), 1.40 (s, 6H). ^{13}C NMR (101 MHz, $CDCl_3$) δ 155.91, 142.95, 140.07, 133.94, 132.49, 131.20, 129.86, 123.31, 121.53, 14.69. HRMS(ESI) calcd. for $C_{19}H_{18}BBrF_2N_2$ [M]: 402.0709; found: 402.0707.

Synthesis of 9. Compound **8** (770 mg, 1.91 mmol, 1 equiv) was dissolved in toluene (25 ml) and 2-(tributylstannyl)pyridine (878 mg, 2.39 mmol, 1.25 equiv) was added under an N_2-atmosphere. $Pd(Ph_3P)_2Cl_2$ (67.0 mg, 0.10 mmol, 0.05 equiv) was added. The reaction mixture was heated to 110 °C for 48 h, cooled to rt, CH_2Cl_2 was added and filtered through celite. It was concentrated and purified with flash column chromatography in CH_2Cl_2 → CH_2Cl_2 + 4 % EtOAc to yield **9** as an orange solid (496 mg, 1.23 mmol, 65%). ^{1}H NMR (400 MHz, $CDCl_3$): δ 8.75 (d, *J* = 4.6 Hz, 1H), 8.18 (d, *J* = 8.1 Hz, 2H), 7.83 (t, *J* = 9.1 Hz, 2H), 7.41 (d, *J* = 8.1 Hz, 2H), 7.30 (t, *J* = 5.3 Hz, 1H), 6.01 (s, 2H), 2.59 (s, 6H), 1.46 (s, 6H). ^{13}C NMR (101 MHz, $CDCl_3$): δ 156.28, 155.59, 149.86, 143.20, 141.35, 139.98, 137.05, 135.67, 131.36, 128.55, 127.57, 122.72, 121.33, 120.65, 14.68. HRMS(ESI) calcd. for $C_{24}H_{23}BF_2N_3^+$ $[M+H]^+$: 402.1948; found: 402.1941.

Synthesis of COP-5-Py. A round-bottom flask was charged with **9** (124 mg, 0.31 mmol, 1 equiv) and $Pd(OAc)_2$ (69.9 mg, 0.31 mmol, 1 equiv). The flask was flushed with nitrogen to create a N_2 atmosphere and protected from light. Benzene (20 mL) was added and the reaction mixture was stirred for 14 h at 50 °C. CH_2Cl_2 was added, it was filtered over celite and concentrated *in vacuo*. 20 mL of a saturated solution of LiCl in acetone was added and stirred at room temperature for 4 h. It was concentrated *in vacuo*, dissolved in CH_2Cl_2, and filtered over celite to remove excess LiCl. It was dissolved in CH_2Cl_2 (10 mL) and pyridine was added (25 uL, 1.2 equiv). COP-5-Py (142 mg, 0.23 mmol, 74%) was obtained by precipitation in hexanes as an orange solid. ^{1}H NMR (500 MHz, $CDCl_3$): δ 9.52 (d, *J* = 5.2 Hz, 1H), 8.85 (d, *J* = 5.0 Hz, 2H), 7.91 – 7.84 (m, 2H), 7.74 (d, *J* = 8.0 Hz, 1H), 7.60 (d, *J* = 7.8 Hz, 1H), 7.47 – 7.42 (m, 2H), 7.23 (t, *J* = 6.6 Hz, 1H), 7.02 (d, *J* = 8.9 Hz, 1H), 6.14 (s, 1H), 5.95 (s, 2H), 2.51 (s, 7H), 1.48 (s, 6H). ^{13}C NMR (126 MHz, $CDCl_3$): δ 165.01, 155.48, 155.12, 153.48, 152.82, 152.55, 146.55, 143.08, 141.92, 139.20, 138.88, 138.75, 136.06, 131.45, 131.19, 126.18, 125.13, 124.56, 123.75, 122.78, 121.25, 118.88, 14.76. HRMS(ESI) calcd. For $C_{31}H_{28}BF_2N_5Pd$ [M+MeCH/-Cl]: 625.1441; found: 625.1435.

Synthesis of 10. A round-bottom flask was charged with methyl 5-(benzyloxycarbonyl)-2,4-dimethylpyrrole-propionate (10.0 g, 31.8 mmol, 1.0 equiv.), palladium on carbon (0.20 g) and acetone (320 mL). A hydrogen atmosphere was established by flushing the flask with hydrogen gas and subsequent attachment of a hydrogen gas containing balloon. Stirring was continued for 12 h at room temperature. Palladium on carbon was filtered off over celite. The reaction mixture was concentrated *in vacuo*, trifluoroacetic acid (32 mL) was added and the reaction mixture was heated to 40 °C for 15 min. The oil bath was removed and $CHCl_3$ was added. The diluted reaction mixture was washed with H_2O and a saturated K_2CO_3 solution in H_2O. The aqueous phases were extracted with $CHCl_3$ and the pooled organic phases were dried over $MgSO_4$ and concentrated *in vacuo*. Purification with flash chromatography on silica gel with CH_2Cl_2 gave **10** (2.8 g, 15.4 mmol,

48%) as a yellow oil. ^{1}H-NMR (400 MHz, $CDCl_3$): δ 8.16 (s, 1H), 6.49 (s, 1H), 3.81 (s, 3H), 2.90 (t, 2H), 2.63 (t, 2H), 2.31 (s, 3H), 2.21 (s, 3H).

Synthesis of 11. A round bottom flask was charged with 4-(Chloromethyl)benzoylchloride (1.46 g, 7.7 mmol, 1 eq). **10** (2.8 g, 15.4 mmol, 2 eq) was dissolved in dry CH_2Cl_2 (30 mL) and added under an N_2-atmosphere. The reaction mixture was stirred for 14 h at room temperature. DIPEA (6.7 mL, 38.5 mmol, 5 eq) was added dropwise and stirred for 20 min. $BF_3{\cdot}OEt_2$ (4.8 mL, 38.5 mmol, 5 eq) was added dropwise and the reaction mixture was stirred for 3 hours. CH_2Cl_2 was added, the organic layer was washed with water, dried over Na_2SO_4 and concentrated in vacuo. The product was purified by flash chromatography on silica gel, eluting with 20% EtOAc, 80% Hexanes → 30% EtOAc, 70% Hexanes. **11** (950 mg, 1.7 mmol, 22%) was obtained as a red solid. ^{1}H-NMR (400 MHz, $CDCl_3$): δ 7.51 (d, 2H), 7.26 (d, 2H), 4.66 (s, 2H), 3.64 (s, 6H), 2.62 (t, 4H), 2.53 (s, 6H), 2.34 (t, 4H), 1.29 (s, 6H). ^{13}C NMR (101 MHz, $CDCl_3$): δ 173.1, 154.4, 140.2, 139.4, 138.7, 135.6, 130.9, 129.4, 128.6, 51.8, 45.7, 34.3, 19.4, 12.7, 12.1. HRMS(ESI) calculated for $[C_{28}H_{32}BClF_2N_2NaO_4]^+$: 567.2004, found: 567.2005.

Synthesis of 12. A round bottom flask was charged with **11** (950 mg, 1.7 mmol, 1 eq), K_2CO_3 (470 mg, 3.4 mmol, 2 eq) and KI (564 mg, 3.4 mmol, 2 eq). CH_3CN (20 mL) and morpholine (741 μL, 8.5 mmol, 5 eq) were added to the flask and the reaction mixture was stirred at 60 °C for 3 h. CH_2Cl_2 was added and the organic layer was extracted with water, dried over Na_2SO_4, and concentrated *in vacuo*. The product was purified by flash chromatography on silica gel, eluting with a 100% hexanes → 100% EtOAc gradient. **12** (968 mg, 1.6 mmol, 94%) was obtained as a red solid. ^{1}H-NMR (400 MHz, $CDCl_3$): δ 7.45 (d, 2H), 7.19 (d, 2H), 3.72 (t, 4H), 3.61 (s, 6H), 3.60 (s, 2H), 2.60 (t, 4H), 2.51 (s, 6H), 2.46 (s, 4H), 2.32 (t, 4H), 1.27 (s, 6H). ^{13}C-NMR (101 MHz, $CDCl_3$): δ 173.07, 154.05, 140.80, 139.36, 134.45, 130.93, 130.04, 129.18, 128.40, 128.13, 66.86, 63.01, 53.49, 51.70, 34.22, 29.72, 19.34, 12.62, 11.90. HRMS(ESI) calculated for $[C_{32}H_{41}BF_2N_3O_5]^+$: 596.3102, found: 596.3104.

Synthesis of COP-3E-Py. A round-bottom flask was charged with **12** (968 mg, 1.6 mmol, 1 eq) and $Pd(OAc)_2$ (347 mg, 1.5 mmol, 0.95 eq). The flask was flushed with nitrogen to create a N_2 atmosphere and protected from light. Benzene (40 mL) was added and the reaction mixture was stirred for 14 h at 50 °C. CH_2Cl_2 was added, it was filtered over celite, and concentrated in vacuo. 60 mL of a saturated solution of LiCl in acetone was added and stirred at room temperature for 4 h. It was concentrated *in vacuo*, dissolved in CH_2Cl_2, and filtered over celite to remove excess LiCl. Hexanes was added and a precipitate was collected with a Büchner funnel. The precipitate was dissolved in CH_2Cl_2. Pyridine (13 μL, 0.15 mmol, 2.2

eq) were added and the solution was stirred for 4 h. Hexanes was added and the precipitate was collected with a Büchner funnel to yield **COP-3E-Py** (90 mg, 0.11 mmol, 70%) as a red solid. ^{1}H-NMR (400 MHz, $CDCl_3$): δ 8.81 (d, 1H), 8.72 (d, 1H), 7.75 (m, 1H), 7.31 (m, 2H), 7.11 (d, 2H), 6.86 (d, 2H), 5.84 (s, 1H), 4.43 (s, 2H) 4.08 (t, 4H), 3.91 (m, 2H) 3.63 (s, 6H), 2.84 (m, 2H), 2.59 (t, 4H), 2.46 (s, 6H), 2.31 (t, 4H), 1.30 (s, 6H). ^{13}C-NMR (101 MHz, $CDCl_3$): δ 173.0, 153.7, 153.4, 153.3, 150.4, 146.6, 141.7, 139.2, 138.7, 138.6, 132.6, 131.0, 130.9, 129.0, 125.5, 125.1, 124.4, 122.7, 68.3, 62.6, 59.0, 51.8, 34.3, 19.4, 12.6, 12.1, 11.9. HRMS(ESI) calculated for [$C_{36}H_{45}BF_2N_5O_5Pd$]: 782.2517, found: 782.2513.

Synthesis of COP-3E-Py'. A round-bottom flask was charged with **COP-3E-Py** (60 mg, 0.073 mmol, 1 eq). CH_2Cl_2 (20 mL) and water (1 mL) were added and the flask was flushed with CO. A CO-filled balloon was attached and the reaction mixture was stirred for 14 h at 31 °C while maintaining an atmosphere of CO. The reaction mixture was cooled to room temperature, transferred to a separatory funnel and diluted with DCM (50 mL). The organic layer was washed with water, dried over sodium sulfate, filtered and concentrated *in vacuo*. The crude product was purified by flash chromatography by elution with a EtOAc → 40% MeOH, 60% EtOAc gradient. **COP-3E-Py'** (43 mg, 6.7 mmol, 92%) was isolated as a red solid. ^{1}H-NMR (400 MHz, $CDCl_3$): δ 8.12 (d, 2H), 7.37 (d, 2H), 3.97 (s, 2H), 3.84 (s, 4H), 3.64 (s, 6H), 2.79 (s, 4H), 2.60 (t, 4H), 2.53 (s, 6H), 2.34 (t, 4H), 1.26 (s, 6H). ^{13}C-NMR (101 MHz, $CDCl_3$): δ 176.3, 173.2, 154.9, 138.9, 138.6, 137.1, 133.7, 132.4, 130.7, 129.7, 65.5, 61.9, 51.9, 51.6, 34.3, 29.8, 20.9, 19.4, 12.8, 12.4. HRMS(ESI) calculated for [$C_{33}H_{41}BF_2N_3O_7$]$^{+}$: 640.3000, found: 640.2995.

X-ray Crystallography. Single crystals were coated with Paratone-N hydrocarbon oil and mounted on Kaptan loops. Temperature was maintained at 100 K with an Oxford Cryostream 700 during data collection at the University of California, Berkeley, College of Chemistry, X-ray Crystallography Facility. Samples were irradiated with Mo-Kα radiation with λ = 0.71073 Å using a Bruker APEX II QUAZAR diffractometer equipped with a Microfocus Sealed Source (Incoatec IμS) and APEX-II detector. The Bruker APEX2 v. 2009.1 software package was used to integrate raw data which were corrected for Lorentz and polarization effects.[86] A semi-empirical absorption correction (SADABS) was applied.[44] Space groups were identified based on systematic absences, E-statistics, and successive refinement of the structures. The structures were solved using direct methods or the Patterson method and refined by least-squares refinement on F^2 and standard difference Fourier techniques using SHELXL.[88–90] Thermal parameters for all non-hydrogen atoms were refined anisotropically, and hydrogen atoms were included at ideal positions and refined isotropically. The ammonium hydrogen in structure COP-1# was located in the electron density map.

Fluorescence Spectroscopy. Fluorescence spectra were recorded on a Photon Technology International Quanta Master 4 L-format scanning spectrofluorometer (Lawrenceville, NJ) equipped with an LPS 220B 75 W xenon lamp and power supply, A 1010B lamp housing with an integrated igniter, switchable 814 photon counting/analog photomultiplier detection unit, and MD5020 motor driver. Samples for emission measurements were contained in a quartz cuvette with a path length of 1 cm and 1.5 mL cell volume (Starna, Atascadero, CA). CO-Probes were dissolved in DMSO (2 mM) and diluted to a final volume of 1 μM in PBS or HEPES (Ca, Mg) buffer. The cuvette was placed in a water bath at 37 °C and after temperature equilibration a t=0 a spectrum was acquired. Subsequently 5 μL of a 10 mM solution of CORM 3 (final concentration: 50 μM) in DMSO was added and the cuvette was again placed in a water bath. Emission spectra were recorded by quickly removing the cuvette from the water bath, recording the spectrum and returning the cuvette to the bath. Spectra were taken at t = 0, 5, 15, 30, 45 and 60 min. COP-3E-Py was excited at 515 nm and emission spectra were recorded from 520 nm to 620 nm in 1 nm intervals with an integration of 0.1. For selectivity assay the CO-Probes were treated with different compounds analogously to the treatment with CORM-3: At 37 °C the tested species were added to a final concentration of 50 μM to a 1 μM aqueous COP solution (PBS (Ca, Mg) buffer). Emission spectra were recorded by quickly removing the cuvette from the water bath, recording the spectrum and returning the cuvette to the bath. Spectra were taken at t = 0, 5, 15, 30, 45 and 60 min. For the selectivity assay, 10 mM solutions of H_2O_2, TBHP, NaOCl, KO_2, $ONOO^-$, H_2S were prepared and 5 μL was added to 1 mL of a 1 μM solution of COP-3E-Py in PBS.

Cell Culture and Confocal Microscopy in Live Cells. Cells were grown in the UC Berkeley Tissue Culturing Facility. HEK293T cells were cultured in Dubelcco's Eagle Medium (DMEM, Invitrogen) supplemented with 10 % fetal bovine serum (FBS, Hyclone) and incubated at 37 °C in 5 % CO_2. One day before imaging, cells were passaged and plated in phenol red-free medium on 8 well chamber slides (Corning, Corning, NY) and grown to 70–80 % (HEK293T) confluency. 100 μL of 3 μM respective CO-Probe in DPBS was prepared from a 0.4 mM COP in DMSO stock solution and added to chambers filled with 200 μL of medium. For CO-response studies in HEK293T cells, 100 μL medium was removed after 60 min of COP incubation and 1.5 μL of 10 mM CORM-3 in DMSO was added (1.5 μL of DMSO for the controls), mixed and readded to the respective chamber. Imaging was performed approximately 120 min after COP addition. Confocal fluorescence microscopy was performed with a Zeiss laser scanning microscope 710 equipped with a 40x water-immersion and 63x oil-immersion objective lens, with Zen 2009 software (Carl Zeiss). COP-1, and COP-1-Py to COP-5-Py were excited at 488 nm and COP-3E-Py was excited at 488 nm or 514 nm. The emission was collected with a META detector. Hoechst 33342 and

ER-Tracker Red E34250 were used at 1 μM concentration and excited at 405 nm. Image analysis was performed using FIJI (National Institute of Health). Co-localization coefficients where calculated with the plugin JACoP.

Detection of CO in Fly Brain Models. Brains were prepared for imaging as previously described.[91] Briefly, brains were dissected in ice cold 0 mM Ca^{2+} HL3 medium (in mM as follows: 70 NaCl, 115 sucrose, 5 KCl, 20 $MgCl_2$, 10 $NaHCO_3$, 5 Trehalose, 5 HEPES, pH 7.3, 359 mOsm), and placed in a recording chamber filled with normal, room temperature HL3 medium (the same recipe as above, containing 1.8 mM $CaCl_2$). COP-3E-Py was added to the buffer from a DMSO stock solution and used at 3 μM final concentration. The antennal lobe (AL) was stimulated (30 pulses, 100 Hz, 1.0 ms pulse duration) using glass micro-electrodes. For NMDA stimulation, 200 μM NMDA, diluted in HL3 containing 4 mM Mg^{2+}, was bath-applied to the recording chamber. Fluorescent imaging was done with a confocal microscope (A1R, Nikon) with a 20x water-immersion lense (numerical aperature 0.5; Nikon). F_0 was obtained by averaging the 5 sequential frames before stimulus onset.

Acknowledgments

We thank the NIH (ES 28096 and ES 4705 to C.J.C.) for funding. J.M. was supported by a fellowship of the German National Academic Foundation (Studienstiftung). D.H. was supported by a fellowship of the Konrad–Adenauer Stiftung. K.J.B. was supported by an NSF graduate fellowship. B.W.M. was supported by an American Heart Association Fellowship. We also thank JSPS KAKENHI for funding (17K07122 to K.U., 19H01013 to M.S., and Takeda Science Foundation to K.U.). We thank Ann Fischer (UC Berkeley Tissue Culture Facility) for expert technical assistance. We thank Allegra Aron, Lakshmi Krishnamoorthy, Joseph A. Cotruvo Jr., Zeming Wang, and Sumin Lee for insightful discussion and experimental assistance.

References

(1) Kim, H. P.; Ryter, S. W.; Choi, A. M. K. Co as a Cellular Signaling Molecule. *Annu. Rev. Pharmacol. Toxicol.* **2006**, *46* (1), 411–449. https://doi.org/10.1146/annurev.pharmtox.46.120604.141053.

(2) Heinemann, S. H.; Hoshi, T.; Westerhausen, M.; Schiller, A. Carbon Monoxide - Physiology, Detection and Controlled Release. *Chem. Commun.* **2014**, *50* (28), 3644–3660. https://doi.org/10.1039/C3CC49196J.

(3) Motterlini, R.; Foresti, R. Biological Signaling by Carbon Monoxide and Carbon Monoxide-Releasing Molecules. *Am. J. Physiol.-Cell Physiol.* **2017**, *312* (3), C302–C313. https://doi.org/10.1152/ajpcell.00360.2016.

(4) Johnson, T. R.; Mann, B. E.; Clark, J. E.; Foresti, R.; Green, C. J.; Motterlini, R. Metal Carbonyls: A New Class of Pharmaceuticals? *Angew. Chem. Int. Ed.* **2003**, *42* (32), 3722–3729. https://doi.org/10.1002/anie.200301634.

(5) Motterlini, R.; Otterbein, L. E. The Therapeutic Potential of Carbon Monoxide. *Nat Rev Drug Discov* **2010**, *9* (9), 728–743. https://doi.org/10.1038/nrd3228.

(6) Mann, B. E. CO-Releasing Molecules: A Personal View. *Organometallics* **2012**, *31* (16), 5728–5735. https://doi.org/10.1021/om300364a.

(7) Clark, J. E.; Foresti, R.; Sarathchandra, P.; Kaur, H.; Green, C. J.; Motterlini, R. Heme Oxygenase-1-Derived Bilirubin Ameliorates Postischemic Myocardial Dysfunction. *Am. J. Physiol.-Heart Circ. Physiol.* **2000**, *278* (2), H643–H651. https://doi.org/10.1152/ajpheart.2000.278.2.H643.

(8) Sato, K.; Balla, J.; Otterbein, L.; Smith, R. N.; Brouard, S.; Lin, Y.; Csizmadia, E.; Sevigny, J.; Robson, S. C.; Vercellotti, G.; Choi, A. M.; Bach, F. H.; Soares, M. P. Carbon Monoxide Generated by Heme Oxygenase-1 Suppresses the Rejection of Mouse-to-Rat Cardiac Transplants. *J. Immunol.* **2001**, *166* (6), 4185–4194. https://doi.org/10.4049/jimmunol.166.6.4185.

(9) Balogun, E.; Hoque, M.; Gong, P.; Killeen, E.; Green, C. J.; Foresti, R.; Alam, J.; Motterlini, R. Curcumin Activates the Haem Oxygenase-1 Gene via Regulation of Nrf2 and the Antioxidant-Responsive Element. *Biochem. J.* **2003**, *371* (3), 887–895. https://doi.org/10.1042/bj20021619.

(10) Matson, J. B.; Webber, M. J.; Tamboli, V. K.; Weber, B.; Stupp, S. I. A Peptide-Based Material for Therapeutic Carbon Monoxide Delivery. *Soft Matter* **2012**, *8* (25), 2689–2692. https://doi.org/10.1039/C2SM25785H.

(11) Zheng, Y.; Ji, X.; Yu, B.; Ji, K.; Gallo, D.; Csizmadia, E.; Zhu, M.; Choudhury, M. R.; Cruz, L. K. C. D. L.; Chittavong, V.; Pan, Z.; Yuan, Z.; Otterbein, L. E.; Wang, B. Enrichment-Triggered Prodrug Activation Demonstrated through Mitochondria-Targeted Delivery of Doxorubicin and Carbon Monoxide. *Nat. Chem.* **2018**, *10* (7), 787–794. https://doi.org/10.1038/s41557-018-0055-2.

(12) Ji, X.; Pan, Z.; Li, C.; Kang, T.; De La Cruz, L. K. C.; Yang, L.; Yuan, Z.; Ke, B.; Wang, B. Esterase-Sensitive and PH-Controlled Carbon Monoxide Prodrugs for Treating Systemic Inflammation. *J. Med. Chem.* **2019**, *62* (6), 3163–3168. https://doi.org/10.1021/acs.jmedchem.9b00073.

(13) Ji, X.; Aghoghovbia, R. E.; De La Cruz, L. K. C.; Pan, Z.; Yang, X.; Yu, B.; Wang, B. Click and Release: A High-Content Bioorthogonal Prodrug with Multiple Outputs. *Org. Lett.* **2019**, *21* (10), 3649–3652. https://doi.org/10.1021/acs.orglett.9b01086.

(14) Kojima, H.; Nakatsubo, N.; Kikuchi, K.; Kawahara, S.; Kirino, Y.; Nagoshi, H.; Hirata, Y.; Nagano, T. Detection and Imaging of Nitric Oxide with Novel Fluorescent Indicators: Diaminofluoresceins. *Anal Chem* **1998**, *70* (13), 2446–2453.

(15) Lim, M. H.; Xu, D.; Lippard, S. J. Visualization of Nitric Oxide in Living Cells by a Copper-Based Fluorescent Probe. *Nat Chem Biol* **2006**, *2* (7), 375–380. https://doi.org/10.1038/nchembio794.

(16) Yang, Y.; Seidlits, S. K.; Adams, M. M.; Lynch, V. M.; Schmidt, C. E.; Anslyn, E. V.; Shear, J. B. A Highly Selective Low-Background Fluorescent Imaging Agent for Nitric Oxide. *J Am Chem Soc* **2010**, *132* (38), 13114–13116. https://doi.org/10.1021/ja1040013.

(17) Lin, V. S.; Chen, W.; Xian, M.; Chang, C. J. Chemical Probes for Molecular Imaging and Detection of Hydrogen Sulfide and Reactive Sulfur Species in Biological Systems. *Chem. Soc. Rev.* **2015**, *44* (14), 4596–4618. https://doi.org/10.1039/C4CS00298A.

(18) Hartle, M. D.; Pluth, M. D. A Practical Guide to Working with H2S at the Interface of Chemistry and Biology. *Chem. Soc. Rev.* **2016**, *45* (22), 6108–6117. https://doi.org/10.1039/C6CS00212A.

(19) Lippert, A. R.; New, E. J.; Chang, C. J. Reaction-Based Fluorescent Probes for Selective Imaging of Hydrogen Sulfide in Living Cells. *J. Am. Chem. Soc.* **2011**, *133* (26), 10078–10080. https://doi.org/10.1021/ja203661j.

(20) Sasakura, K.; Hanaoka, K.; Shibuya, N.; Mikami, Y.; Kimura, Y.; Komatsu, T.; Ueno, T.; Terai, T.; Kimura, H.; Nagano, T. Development of a Highly Selective Fluorescence Probe for Hydrogen Sulfide. *J Am Chem Soc* **2011**, *133* (45), 18003–18005. https://doi.org/10.1021/ja207851s.

(21) Peng, H.; Cheng, Y.; Dai, C.; King, A. L.; Predmore, B. L.; Lefer, D. J.; Wang, B. A Fluorescent Probe for Fast and Quantitative Detection of Hydrogen Sulfide in Blood. *Angew. Chem. Int. Ed.* **2011**, *50* (41), 9672–9675. https://doi.org/10.1002/anie.201104236.

(22) Montoya, L. A.; Pluth, M. D. Selective Turn-on Fluorescent Probes for Imaging Hydrogen Sulfide in Living Cells. *Chem. Commun.* **2012**, *48* (39), 4767–4769. https://doi.org/10.1039/C2CC30730H.

(23) Lin, V. S.; Lippert, A. R.; Chang, C. J. Cell-Trappable Fluorescent Probes for Endogenous Hydrogen Sulfide Signaling and Imaging H2O2-Dependent H2S Production. *Proc Natl Acad Sci U A* **2013**, *110* (18), 7131–7135. https://doi.org/10.1073/pnas.1302193110.

(24) Henthorn, H. A.; Pluth, M. D. Mechanistic Insights into the H2S-Mediated Reduction of Aryl Azides Commonly Used in H2S Detection. *J. Am. Chem. Soc.* **2015**, *137* (48), 15330–15336. https://doi.org/10.1021/jacs.5b10675.

(25) Cao, J.; Lopez, R.; Thacker, J. M.; Moon, J. Y.; Jiang, C.; Morris, S. N. S.; Bauer, J. H.; Tao, P.; Mason, R. P.; Lippert, A. R. Chemiluminescent Probes for Imaging H2S in Living Animals. *Chem. Sci.* **2015**, *6* (3), 1979–1985. https://doi.org/10.1039/C4SC03516J.

(26) Steiger, A. K.; Pardue, S.; Kevil, C. G.; Pluth, M. D. Self-Immolative Thiocarbamates Provide Access to Triggered H2S Donors and Analyte Replacement Fluorescent Probes. *J. Am. Chem. Soc.* **2016**, *138* (23), 7256–7259. https://doi.org/10.1021/jacs.6b03780.

(27) Chen, W.; Pacheco, A.; Takano, Y.; Day, J. J.; Hanaoka, K.; Xian, M. A Single Fluorescent Probe to Visualize Hydrogen Sulfide and Hydrogen Polysulfides with Different Fluorescence Signals. *Angew. Chem. Int. Ed.* **2016**, *55* (34), 9993–9996. https://doi.org/10.1002/anie.201604892.

(28) Lippert, A. R.; Van de Bittner, G. C.; Chang, C. J. Boronate Oxidation as a Bioorthogonal Reaction Approach for Studying the Chemistry of Hydrogen Peroxide in Living Systems. *Acc Chem Res* **2011**, *44* (9), 793–804. https://doi.org/10.1021/ar200126t.

(29) Brewer, T. F.; Garcia, F. J.; Onak, C. S.; Carroll, K. S.; Chang, C. J. Chemical Approaches to Discovery and Study of Sources and Targets of Hydrogen Peroxide Redox Signaling Through NADPH Oxidase Proteins. *Annu. Rev. Biochem.* **2015**, *84* (1), 765–790. https://doi.org/10.1146/annurev-biochem-060614-034018.

(30) Chang, M. C. Y.; Pralle, A.; Isacoff, E. Y.; Chang, C. J. A Selective, Cell-Permeable Optical Probe for Hydrogen Peroxide in Living Cells. *J. Am. Chem. Soc.* **2004**, *126* (47), 15392–15393. https://doi.org/10.1021/ja0441716.

(31) Miller, E. W.; Albers, A. E.; Pralle, A.; Isacoff, E. Y.; Chang, C. J. Boronate-Based Fluorescent Probes for Imaging Cellular Hydrogen Peroxide. *J. Am. Chem. Soc.* **2005**, *127* (47), 16652–16659. https://doi.org/10.1021/ja054474f.

(32) Dickinson, B. C.; Chang, C. J. A Targetable Fluorescent Probe for Imaging Hydrogen Peroxide in the Mitochondria of Living Cells. *J. Am. Chem. Soc.* **2008**, *130* (30), 9638–9639. https://doi.org/10.1021/ja802355u.

(33) Srikun, D.; Miller, E. W.; Domaille, D. W.; Chang, C. J. An ICT-Based Approach to Ratiometric Fluorescence Imaging of Hydrogen Peroxide Produced in Living Cells. *J Am Chem Soc* **2008**, *130* (14), 4596–4597. https://doi.org/10.1021/ja711480f.

(34) Miller, E. W.; Dickinson, B. C.; Chang, C. J. Aquaporin-3 Mediates Hydrogen Peroxide Uptake to Regulate Downstream Intracellular Signaling. *Proc Natl Acad Sci U A* **2010**, *107* (36), 15681–15686. https://doi.org/10.1073/pnas.1005776107.

(35) Bittner, G. C. V. de; Dubikovskaya, E. A.; Bertozzi, C. R.; Chang, C. J. In Vivo Imaging of Hydrogen Peroxide Production in a Murine Tumor Model with a Chemoselective Bioluminescent Reporter. *Proc. Natl. Acad. Sci.* **2010**, *107* (50), 21316–21321. https://doi.org/10.1073/pnas.1012864107.

(36) Srikun, D.; Albers, A. E.; Nam, C. I.; Iavarone, A. T.; Chang, C. J. Organelle-Targetable Fluorescent Probes for Imaging Hydrogen Peroxide in Living Cells via SNAP-Tag Protein Labeling. *J Am Chem Soc* **2010**, *132* (12), 4455–4465. https://doi.org/10.1021/ja100117u.

(37) Karton-Lifshin, N.; Segal, E.; Omer, L.; Portnoy, M.; Satchi-Fainaro, R.; Shabat, D. A Unique Paradigm for a Turn-ON Near-Infrared Cyanine-Based Probe: Noninvasive Intravital Optical Imaging of Hydrogen Peroxide. *J. Am. Chem. Soc.* **2011**, *133* (28), 10960–10965. https://doi.org/10.1021/ja203145v.

(38) Abo, M.; Urano, Y.; Hanaoka, K.; Terai, T.; Komatsu, T.; Nagano, T. Development of a Highly Sensitive Fluorescence Probe for Hydrogen Peroxide. *J. Am. Chem. Soc.* **2011**, *133* (27), 10629–10637. https://doi.org/10.1021/ja203521e.

(39) Hitomi, Y.; Takeyasu, T.; Kodera, M. Iron Complex-Based Fluorescent Probes for Intracellular Hydrogen Peroxide Detection. *Chem. Commun.* **2013**, *49* (85), 9929–9931. https://doi.org/10.1039/C3CC44471F.

(40) Guo, H.; Aleyasin, H.; Dickinson, B. C.; Haskew-Layton, R. E.; Ratan, R. R. Recent Advances in Hydrogen Peroxide Imaging for Biological Applications. *Cell Biosci* **2014**, *4* (1), 64. https://doi.org/10.1186/2045-3701-4-64.

(41) Carroll, V.; Michel, B. W.; Blecha, J.; VanBrocklin, H.; Keshari, K.; Wilson, D.; Chang, C. J. A Boronate-Caged [18F]FLT Probe for Hydrogen Peroxide Detection Using Positron Emission Tomography. *J. Am. Chem. Soc.* **2014**, *136* (42), 14742–14745. https://doi.org/10.1021/ja509198w.

(42) Green, O.; Gnaim, S.; Blau, R.; Eldar-Boock, A.; Satchi-Fainaro, R.; Shabat, D. Near-Infrared Dioxetane Luminophores with Direct Chemiluminescence Emission Mode. *J. Am. Chem. Soc.* **2017**, *139* (37), 13243–13248. https://doi.org/10.1021/jacs.7b08446.

(43) Ye, S.; Hu, J. J.; Yang, D. Tandem Payne/Dakin Reaction: A New Strategy for Hydrogen Peroxide Detection and Molecular Imaging. *Angew. Chem. Int. Ed.* **2018**, *57* (32), 10173–10177. https://doi.org/10.1002/anie.201805162.

(44) Chan, J.; Dodani, S. C.; Chang, C. J. Reaction-Based Small-Molecule Fluorescent Probes for Chemoselective Bioimaging. *Nat. Chem.* **2012**, *4* (12), 973–984. https://doi.org/10.1038/nchem.1500.

(45) Yang, Y.; Zhao, Q.; Feng, W.; Li, F. Luminescent Chemodosimeters for Bioimaging. *Chem. Rev.* **2013**, *113* (1), 192–270. https://doi.org/10.1021/cr2004103.

(46) Tang, Y.; Lee, D.; Wang, J.; Li, G.; Yu, J.; Lin, W.; Yoon, J. Development of Fluorescent Probes Based on Protection–Deprotection of the Key Functional Groups for Biological Imaging. *Chem. Soc. Rev.* **2015**, *44* (15), 5003–5015. https://doi.org/10.1039/C5CS00103J.

(47) Wu, D.; Sedgwick, A. C.; Gunnlaugsson, T.; Akkaya, E. U.; Yoon, J.; James, T. D. Fluorescent Chemosensors: The Past, Present and Future. *Chem. Soc. Rev.* **2017**, *46* (23), 7105–7123. https://doi.org/10.1039/C7CS00240H.

(48) Bruemmer, K. J.; Crossley, S. W. M.; Chang, C. J. Activity-Based Sensing: A Synthetic Methods Approach for Selective Molecular Imaging and Beyond. *Angew. Chem. Int. Ed. n/a* (n/a). https://doi.org/10.1002/anie.201909690.

(49) Tang, Y.; Ma, Y.; Yin, J.; Lin, W. Strategies for Designing Organic Fluorescent Probes for Biological Imaging of Reactive Carbonyl Species. *Chem. Soc. Rev.* **2019**, *48* (15), 4036–4048. https://doi.org/10.1039/C8CS00956B.

(50) Ohata, J.; Bruemmer, K. J.; Chang, C. J. Activity-Based Sensing Methods for Monitoring the Reactive Carbon Species Carbon Monoxide and Formaldehyde in Living Systems. *Acc. Chem. Res.* **2019**, *52* (10), 2841–2848. https://doi.org/10.1021/acs.accounts.9b00386.

(51) Yang, M.; Fan, J.; Du, J.; Peng, X. Small-Molecule Fluorescent Probes for Imaging Gaseous Signaling Molecules: Current Progress and Future Implication. *Chem. Sci.* **2020**. https://doi.org/10.1039/D0SC01482F.

(52) Michel, B. W.; Lippert, A. R.; Chang, C. J. A Reaction-Based Fluorescent Probe for Selective Imaging of Carbon Monoxide in Living Cells Using a Palladium-Mediated Carbonylation. *J. Am. Chem. Soc.* **2012**, *134* (38), 15668–15671. https://doi.org/10.1021/ja307017b.

(53) Wang, J.; Karpus, J.; Zhao, B. S.; Luo, Z.; Chen, P. R.; He, C. A Selective Fluorescent Probe for Carbon Monoxide Imaging in Living Cells. *Angew. Chem. Int. Ed.* **2012**, *51* (38), 9652–9656. https://doi.org/10.1002/anie.201203684.

(54) Wilson, J. L.; Fayad Kobeissi, S.; Oudir, S.; Haas, B.; Michel, B.; Dubois Randé, J.-L.; Ollivier, A.; Martens, T.; Rivard, M.; Motterlini, R.; Foresti, R. Design and Synthesis of New Hybrid Molecules That Activate the Transcription Factor Nrf2 and Simultaneously Release Carbon Monoxide. *Chem. – Eur. J.* **2014**, *20* (45), 14698–14704. https://doi.org/10.1002/chem.201403901.

(55) Chaves-Ferreira, M.; Albuquerque, I. S.; Matak-Vinkovic, D.; Coelho, A. C.; Carvalho, S. M.; Saraiva, L. M.; Romão, C. C.; Bernardes, G. J. L. Spontaneous CO Release from RuII(CO)2–Protein Complexes in Aqueous Solution, Cells, and Mice. *Angew. Chem. Int. Ed.* **2014**, n/a-n/a. https://doi.org/10.1002/anie.201409344.

(56) Fujita, K.; Tanaka, Y.; Sho, T.; Ozeki, S.; Abe, S.; Hikage, T.; Kuchimaru, T.; Kizaka-Kondoh, S.; Ueno, T. Intracellular CO Release from Composite of Ferritin and Ruthenium Carbonyl Complexes. *J. Am. Chem. Soc.* **2014**, *136* (48), 16902–16908. https://doi.org/10.1021/ja508938f.

(57) Albuquerque, I. S.; Jeremias, H. F.; Chaves-Ferreira, M.; Matak-Vinkovic, D.; Boutureira, O.; Romao, C. C.; Bernardes, G. J. L. An Artificial CO-Releasing Metalloprotein Built by Histidine-Selective Metallation. *Chem. Commun.* **2015**, *51* (19), 3993–3996. https://doi.org/10.1039/C4CC10204E.

(58) Li, Y.; Wang, X.; Yang, J.; Xie, X.; Li, M.; Niu, J.; Tong, L.; Tang, B. Fluorescent Probe Based on Azobenzene-Cyclopalladium for the Selective Imaging of Endogenous Carbon Monoxide under Hypoxia Conditions. *Anal. Chem.* **2016**, *88* (22), 11154–11159. https://doi.org/10.1021/acs.analchem.6b03376.

(59) Liu, K.; Kong, X.; Ma, Y.; Lin, W. Preparation of a Nile Red–Pd-Based Fluorescent CO Probe and Its Imaging Applications *in Vitro* and *in Vivo*. *Nat. Protoc.* **2018**, *13* (5), 1020–1033. https://doi.org/10.1038/nprot.2018.013.

(60) Sun, M.; Yu, H.; Zhang, K.; Wang, S.; Hayat, T.; Alsaedi, A.; Huang, D. Palladacycle Based Fluorescence Turn-On Probe for Sensitive Detection of Carbon Monoxide. *ACS Sens.* **2018**, *3* (2), 285–289. https://doi.org/10.1021/acssensors.7b00835.

(61) Xu, S.; Liu, H.-W.; Yin, X.; Yuan, L.; Huan, S.-Y.; Zhang, X.-B. A Cell Membrane-Anchored Fluorescent Probe for Monitoring Carbon Monoxide Release from Living Cells. *Chem. Sci.* **2019**, *10* (1), 320–325. https://doi.org/10.1039/C8SC03584A.

(62) Zheng, K.; Lin, W.; Tan, L.; Chen, H.; Cui, H. A Unique Carbazole-Coumarin Fused Two-Photon Platform: Development of a Robust Two-Photon Fluorescent Probe for Imaging Carbon Monoxide in Living Tissues. *Chem. Sci.* **2014**, *5* (9), 3439–3448. https://doi.org/10.1039/C4SC00283K.

(63) Cao, Y.; Li, D.-W.; Zhao, L.-J.; Liu, X.-Y.; Cao, X.-M.; Long, Y.-T. Highly Selective Detection of Carbon Monoxide in Living Cells by Palladacycle Carbonylation-Based Surface Enhanced Raman Spectroscopy Nanosensors. *Anal. Chem.* **2015**, *87* (19), 9696–9701. https://doi.org/10.1021/acs.analchem.5b01793.

(64) Xu, M.; Liu, L.; Hu, J.; Zhao, Y.; Yan, Q. CO-Signaling Molecule-Responsive Nanoparticles Formed from Palladium-Containing Block Copolymers. *ACS Macro Lett.* **2017**, *6* (4), 458–462. https://doi.org/10.1021/acsmacrolett.7b00042.

(65) Pal, S.; Mukherjee, M.; Sen, B.; Mandal, S. K.; Lohar, S.; Chattopadhyay, P.; Dhara, K. A New Fluorogenic Probe for the Selective Detection of Carbon Monoxide in Aqueous Medium Based on Pd(0) Mediated Reaction. *Chem. Commun.* **2015**, *51* (21), 4410–4413. https://doi.org/10.1039/C5CC00902B.

(66) Yan, J.; Zhu, J.; Tan, Q.; Zhou, L.; Yao, P.; Lu, Y.; Tan, J.; Zhang, L. Development of a Colorimetric and NIR Fluorescent Dual Probe for Carbon Monoxide. *RSC Adv.* **2016**, *6* (70), 65373–65376. https://doi.org/10.1039/C6RA14409H.

(67) Feng, S.; Liu, D.; Feng, W.; Feng, G. Allyl Fluorescein Ethers as Promising Fluorescent Probes for Carbon Monoxide Imaging in Living Cells. *Anal. Chem.* **2017**, *89* (6), 3754–3760. https://doi.org/10.1021/acs.analchem.7b00135.

(68) Chankeshwara, S. V.; Indrigo, E.; Bradley, M. Palladium-Mediated Chemistry in Living Cells. *Curr. Opin. Chem. Biol.* **8**, *21*, 128–135. https://doi.org/10.1016/j.cbpa.2014.07.007.

(69) Iovan, D. A.; Jia, S.; Chang, C. J. Inorganic Chemistry Approaches to Activity-Based Sensing: From Metal Sensors to Bioorthogonal Metal Chemistry. *Inorg. Chem.* **2019**, *58* (20), 13546–13560. https://doi.org/10.1021/acs.inorgchem.9b01221.

(70) Garner, A. L.; Koide, K. Fluorescent Method for Platinum Detection in Buffers and Serums for Cancer Medicine and Occupational Hazards. *Chem. Commun.* **2008**, No. 1, 83–85. https://doi.org/10.1039/B817220J.

(71) Yuan, L.; Lin, W.; Tan, L.; Zheng, K.; Huang, W. Lighting up Carbon Monoxide: Fluorescent Probes for Monitoring CO in Living Cells. *Angew. Chem. Int. Ed.* **2013**, *52* (6), 1628–1630. https://doi.org/10.1002/anie.201208346.

(72) Li, J.; Yu, J.; Zhao, J.; Wang, J.; Zheng, S.; Lin, S.; Chen, L.; Yang, M.; Jia, S.; Zhang, X.; Chen, P. R. Palladium-Triggered Deprotection Chemistry for Protein Activation in Living Cells. *Nat. Chem.* **2014**, *6* (4), 352–361. https://doi.org/10.1038/nchem.1887.

(73) Li, X.; Gao, X.; Shi, W.; Ma, H. Design Strategies for Water-Soluble Small Molecular Chromogenic and Fluorogenic Probes. *Chem. Rev.* **2014**, *114* (1), 590–659. https://doi.org/10.1021/cr300508p.

(74) Soldevila-Barreda, J. J.; Romero-Canelón, I.; Habtemariam, A.; Sadler, P. J. Transfer Hydrogenation Catalysis in Cells as a New Approach to Anticancer Drug Design. *Nat. Commun.* **2015**, *6* (1), 1–9. https://doi.org/10.1038/ncomms7582.

(75) Bose, S.; Ngo, A. H.; Do, L. H. Intracellular Transfer Hydrogenation Mediated by Unprotected Organoiridium Catalysts. *J. Am. Chem. Soc.* **2017**, *139* (26), 8792–8795. https://doi.org/10.1021/jacs.7b03872.

(76) Indrigo, E.; Clavadetscher, J.; V. Chankeshwara, S.; Megia-Fernandez, A.; Lilienkampf, A.; Bradley, M. Intracellular Delivery of a Catalytic Organometallic Complex. *Chem. Commun.* **2017**, *53* (50), 6712–6715. https://doi.org/10.1039/C7CC02988H.

(77) Toussaint, S. N. W.; Calkins, R. T.; Lee, S.; Michel, B. W. Olefin Metathesis-Based Fluorescent Probes for the Selective Detection of Ethylene in Live Cells. *J. Am. Chem. Soc.* **2018**, *140* (41), 13151–13155. https://doi.org/10.1021/jacs.8b05191.

(78) Pierzyńska-Mach, A.; Janowski, P. A.; Dobrucki, J. W. Evaluation of Acridine Orange, LysoTracker Red, and Quinacrine as Fluorescent Probes for Long-Term Tracking of Acidic Vesicles. *Cytometry A* **2014**, *85* (8), 729–737. https://doi.org/10.1002/cyto.a.22495.

(79) Dupont, J.; Consorti, C. S.; Spencer, J. The Potential of Palladacycles: More Than Just Precatalysts. *Chem. Rev.* **2005**, *105* (6), 2527–2572. https://doi.org/10.1021/cr030681r.

(80) Dupont, Jairton.; Pfeffer, Michel.; Daran, J. Claude.; Jeannin, Yves. Reactivity of Cyclopalladated Compounds. Part 17. Influence of the Donor Atom in Metallacyclic Rings on the Insertion of Tert-Butyl Isocyanide and Carbon Monoxide into Their Palladium-Carbon Bonds. X-Ray Molecular Structure of Cyclo-[Pd(.Eta.-(CN)-.Mu.-C(C6H4CH2SMe):NBu-Tert)Br]2. *Organometallics* **1987**, *6* (4), 899–901. https://doi.org/10.1021/om00147a041.

(81) Tsien, R. Y. A Non-Disruptive Technique for Loading Calcium Buffers and Indicators into Cells. *Nature* **1981**, *290* (5806), 527–528. https://doi.org/10.1038/290527a0.

(82) Ryter, S. W.; Alam, J.; Choi, A. M. K. *Heme Oxygenase-1/Carbon Monoxide: From Basic Science to Therapeutic Applications*; 2006; Vol. 86. https://doi.org/10.1152/physrev.00011.2005.

(83) Ueno, K.; Morstein, J.; Ofusa, K.; Naganos, S.; Suzuki-Sawano, E.; Minegishi, S.; Rezgui, S. P.; Kitagishi, H.; Michel, B. W.; Chang, C. J.; Horiuchi, J.; Saitoe, M. "Carbon Monoxide, a Retrograde Messenger Generated in Post-Synaptic Mushroom Body Neurons Evokes Non-Canonical Dopamine Release." *J. Neurosci.* **2020**. https://doi.org/10.1523/JNEUROSCI.2378-19.2020.

(84) Clark, J. E.; Naughton, P.; Shurey, S.; Green, C. J.; Johnson, T. R.; Mann, B. E.; Foresti, R.; Motterlini, R. Cardioprotective Actions by a Water-Soluble Carbon Monoxide–Releasing Molecule. *Circ. Res.* **2003**, *93* (2), e2–e8. https://doi.org/10.1161/01.res.0000084381.86567.08.

(85) Isaad, J.; El Achari, A. BODIPY Modified Silica Coated Magnetite Nanoparticles as Fluorescent Hybrid Material for Cu (II) Detection in Aqueous Medium. *Dyes Pigments* **2013**, *99* (3), 878–886. https://doi.org/10.1016/j.dyepig.2013.07.031.

(86) APEX2, v. 2009; Bruker Analytical X-Ray Systems, Inc: Madison, WI, 2009.

(87) G. M. Sheldrick, SADABS, version 2.03; Bruker Analytical X-RaySystems, Madison, WI, 2000.

(88) Sheldrick, G. M. Phase Annealing in SHELX-90: Direct Methods for Larger Structures. *Acta Crystallogr. A* **1990**, *46* (6), 467–473. https://doi.org/10.1107/S0108767390000277.

(89) Sheldrick, G. M. A Short History of SHELX. *Acta Crystallogr. A* **2008**, *64* (1), 112–122. https://doi.org/10.1107/S0108767307043930.

(90) G. M. Sheldrick, SHELXL-97: Program for crystal structure determination, University of Göttingen: Göttingen, Germany, 1997.

(91) Ueno, K.; Naganos, S.; Hirano, Y.; Horiuchi, J.; Saitoe, M. Long-Term Enhancement of Synaptic Transmission between Antennal Lobe and Mushroom Body in Cultured Drosophila Brain. *J. Physiol.* **2013**, *591* (1), 287–302. https://doi.org/10.1113/jphysiol.2012.242909.

TOC Figure

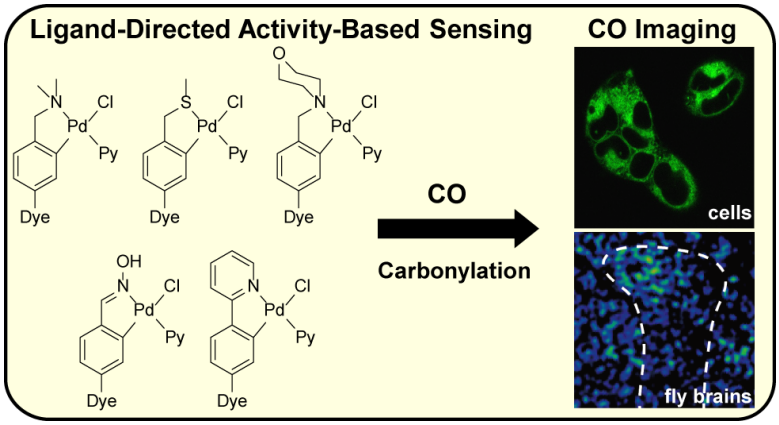
Ligand-Directed Activity-Based Sensing
CO Imaging
CO
Carbonylation
cells
fly brains
Dye
Pd
Cl
Py
N
S
O
OH